Monomeric and Dimeric Oxidomolybdenum(V and VI) Complexes, Cytotoxicity, and DNA Interaction Studies: Molybdenum Assisted C=N Bond Cleavage of Salophen Ligands

Sudarshana Majumder,[†] Sagarika Pasayat,[†] Alok K. Panda,[‡] Subhashree P. Dash,[†,§] Satabdi Roy,[†] Ashis Biswas,[‡] Mokshada E. Varma,[||] Bimba N. Joshi,[||] Eugenio Garribba,[⊥] Chahat Kausar,[#] Samir Kumar Patra,[#] Werner Kaminsky,[¶] Aurélien Crochet,[¥] and Rupam Dinda[*,†]

[†]Department of Chemistry, National Institute of Technology, Rourkela 769008, Odisha, India
[‡]School of Basic Sciences, Indian Institute of Technology Bhubaneswar, Bhubaneswar 751013, Odisha, India
[§]Department of Basic Sciences, Paralamaharaja Engineering College, Sitalapalli, Brahmapur, Odisha 761003, India
[||]Bioprospecting Group, Agharkar Research Institute, G.G. Agharkar Road, Pune 411004, India
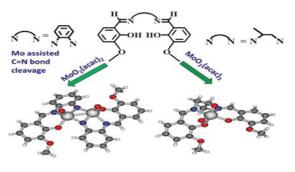[⊥]Dipartimento di Chimica e Farmacia, Università di Sassari, Via Vienna 2, I-07100 Sassari, Italy
[#]Department of Life Science, National Institute of Technology, Rourkela 769008, Odisha, India
[¶]Department of Chemistry, University of Washington, Box 351700, Seattle, Washington 98195, United States
[¥]Department of Chemistry, Fribourg Center for Nanomaterials, University of Fribourg, CH-1700 Fribourg, Switzerland

Ⓢ *Supporting Information*

ABSTRACT: Four novel dimeric bis-μ-imido bridged metal−metal bonded oxidomolybdenum(V) complexes $[Mo^V_2O_2L'^{1-4}_2]$ (**1−4**) (where L'^{1-4} are rearranged ligands formed *in situ* from H_2L^{1-4}) and a new mononuclear dioxidomolybdenum(VI) complex $[Mo^{VI}O_2L^5]$ (**5**) synthesized from salen type N_2O_2 ligands are reported. This rare series of imido-bridged complexes (**1−4**) have been furnished from rearranged $H_3L'^{1-4}$ ligands, containing an aromatic diimine (*o*-phenylenediamine) "linker", where Mo assisted hydrolysis followed by −C=N bond cleavage of one of the arms of the ligand H_2L^{1-4} took place. A monomeric molybdenum(V) intermediate species $[Mo^VO-(HL'^{1-4})(OEt)]$ (I_d^{1-4}) was generated *in situ*. The concomitant deprotonation and dimerization of two molybdenum(V) intermediate species (I_d^{1-4}) ultimately resulted in the formation of a bis-μ-imido bridge between the two molybdenum centers of $[Mo^V_2O_2L'^{1-4}_2]$ (**1−4**). The mechanism of formation of **1−4** has been discussed, and one of the rare intermediate monomeric molybdenum(V) species I_d^4 has been isolated in the solid state and characterized. The monomeric dioxidomolybdenum(VI) complex $[Mo^{VI}O_2L^5]$ (**5**) was prepared from the ligand H_2L^5 where the aromatic "linker" was replaced by an aliphatic diimine (1,2-diaminopropane). All the ligands and complexes have been characterized by elemental analysis, IR, UV−vis spectroscopy, NMR, ESI-MS, and cyclic voltammetry, and the structural features of **1**, **2**, **4**, and **5** have been solved by X-ray crystallography. The DNA binding and cleavage activity of **1−5** have been explored. The complexes interact with CT-DNA by the groove binding mode, and the binding constants range between 10^3 and 10^4 M^{-1}. Fairly good photoinduced cleavage of pUC19 supercoiled plasmid DNA was exhibited by all the complexes, with **4** showing the most promising photoinduced DNA cleavage activity of ∼93%. Moreover, *in vitro* cytotoxic activity of all the complexes was evaluated by MTT assay, which reveals that the complexes induce cell death in MCF-7 (human breast adenocarcinoma) and HCT-15 (colon cancer) cell lines.

INTRODUCTION

The interesting coordination behavior and structural integrity of metal−metal bonded molybdenum(V) complexes make their chemistry a subject of enthusiastic research.[1,2] In the past two decades, there have been extensive studies on binuclear and polynuclear molybdenum(V) complexes containing metal−metal bonds, where molybdenum is found to be bridged through oxido,[3] sulfido,[4] telluro,[5] chloride,[6] or methoxido[7] functionalities and the d-electrons of the Mo[V] center are localized into Mo[V]−Mo[V] single bonds.[8] However, examples of bis-μ-imido bridged metal−metal bonded oxidomolybdenum-(V) complexes are few in the literature[9] although molybdenum-(V) complexes with terminal imide groups[10] have been long known.

On the other hand, despite the tremendous success of platinum anticancer drugs,[11,12] there is an acute need for the development of alternative chemotherapeutic agents in cancer therapy, due to the severe side effects and resistance phenomena of the established drugs.[13−16] Generally anticancer agents which damage or block DNA synthesis are approved for clinical use.[17] In this regard, the oxidative nature of metal complexes of salens have encouraged biochemists to develop novel DNA/RNA modifiers as well as biomolecular probes.[18−21] It has been established that the DNA interaction and antiproliferative potential of the metallo−salen complexes depend on the type of the central metal and the position and nature of the substituents present on the salen moiety.[18,21,22] In addition, the bridging aliphatic or aromatic diimine moiety of salen type ligands has also been reported to significantly influence their cytotoxic efficiencies.[22a,d,23]

In recent times, the studies on DNA interactions and antiproliferative activities of molybdenum complexes have gained substantial interest.[24−34] However, structural reports on oxidomolybdenum complexes with salen type ligands are few[35−37] and their pharmacological properties remain practically unexplored.

Our research group has been involved in the synthetic, structural, and biological studies of transition metal complexes in the recent few years.[38] In continuation of our research, herein we have reported four novel dimeric bis-μ-imido bridged metal−metal bonded oxidomolybdenum(V) complexes $[Mo_2^VO_2L'_2^{1−4}]$ (**1−4**) (where $L'^{1−4}$ are rearranged ligands; discussed later) and a new monomeric dioxidomolybdenum-(VI) complex $[Mo^{VI}O_2L^5]$ (**5**) synthesized from salen type N_2O_2 ligands. As the site specific imine reduction of salen type ligands is quite unusual in the literature[39] and it has been reported that molybdenum assisted reduction of aromatic imines is more feasible than that of aliphatic imines,[40] in this work an aromatic and an aliphatic diamine were judiciously chosen for preparing ligands to study their influence on the control of molecular structure of oxidomolybdenum complexes, as well as to investigate their impact on DNA interactions and cytotoxicity studies. It was observed that, during metalation with $MoO_2(acac)_2$, the salophen ligands $H_2L^{1−4}$ containing the aromatic diimine bridges transformed to new rearranged ligands $H_3L'^{1−4}$ through molybdenum assisted hydrolysis followed by −C=N bond cleavage of one of the arms of the salophen ligands. The corresponding molybdenum(V) intermediate $[Mo^VO(HL'^{1−4})(OEt)]$ ($I_d^{1−4}$) was generated from an initially formed dioxidomolybdenum(VI) species $[Mo^{VI}O_2(HL^{1−4})(EtOH)(acac)]$ ($I^{1−4}$) during the course of the reaction (one of the molybdenum(V) intermediate species I_d^4 has been isolated and characterized). Finally, the molybdenum(V) intermediate ($I_d^{1−4}$) underwent deprotonation and concomitant dimerization to form bis-μ-imido bridged metal−metal bonded oxidomolybdenum(V) complexes $[Mo_2^VO_2L'_2^{1−4}]$ (**1−4**). In contrast, the ligand H_2L^5 with an aliphatic imine component produced a simple dioxidomolybdenum(VI) complex $[Mo^{VI}O_2L^5]$ (**5**) where no such ligand rearrangement took place. The key role of molybdenum in the ligand transformation can be elucidated by taking into account the reports of several other transition metal complexes[41] using similar ligands, where no such −C=N bond cleavage takes place.

All the ligands and complexes have been characterized by various physicochemical techniques, and the structural features of **1**, **2**, **4**, and **5** have been solved by X-ray crystallography. It is relevant to mention that, to the best of our knowledge, this is the first report of some bis-μ-imido bridged dimeric oxidomolybdenum(V) complexes $[Mo_2^VO_2L'_2^{1−4}]$ (**1−4**) synthesized from partially reduced salophen ligands, which have been structurally characterized. **1−5** were tested for their potential of exhibiting DNA binding and cleavage activity, and their *in vitro* antiproliferative activity was assayed against the MCF-7 and HCT-15 cell lines.

■ EXPERIMENTAL SECTION

Materials and Methods. All chemicals were procured commercially and used as received. $[MoO_2(acac)_2]$ was synthesized according to a reported procedure.[42] A Vario EL cube CHNS elemental analyzer was used for elemental analysis measurement. A PerkinElmer Spectrum RX I spectrophotometer was employed for recording IR spectra. A Bruker Ultrashield 400 MHz spectrometer was used for measuring ^1H and ^{13}C NMR spectra where $SiMe_4$ was used as the internal standard. A PerkinElmer Lambda 25 spectrophotometer was employed to measure the electronic spectra. A Sherwood Scientific AUTOMSB sample magnetometer was used for measuring magnetic susceptibility. Conductivity was measured with a Eutech CON 700 conductivity meter. ESI-MS were recorded on a SQ-300 MS instrument operating in ESI mode. Electrochemical data were recorded using a CH-Instruments (model no. CHI6003E) electrochemical analyzer. The cyclic voltammetry experiments were performed using Pt working and auxiliary electrodes, SCE as reference electrode, and TBAP as supporting electrolyte. TBAP (tetrabutylammonium perchlorate) was purchased from commercial sources, dried properly, and used as a supporting electrolyte for cyclic voltammetry experiments. EPR spectra were recorded from 0 to 8000 G at 298 K (room temperature) with an X-band (9.4 GHz) Bruker EMX spectrometer equipped with an HP 53150A microwave frequency counter; the microwave frequency used was in the range 9.40−9.41 GHz. The supercoiled (SC) pUC19 DNA from *Escherichia coli* DH5α cells was purified by using a GeneJET Plasmid Isolation Kit (Thermo Scientific, USA). Calf thymus (CT) DNA (biochemistry grade) was procured from SRL (India). Agarose (molecular biology grade) was procured from Sigma-Aldrich (USA). MCF-7 (human breast adenocarcinoma cell line), HCT-15 (colon cancer cell line), and HaCaT (immortalized human keratinocytes) were purchased from NCCS, Pune. Penicillin, streptomycin, DMEM, and fetal bovine serum were procured from Invitrogen, and MTT was procured from Spectrochem. Propidium iodide was purchased from Sigma-Aldrich (USA). *Caution! Although no difficulties were encountered during the course of this work, attention is drawn to the potentially hazardous nature of perchlorates.*

Synthesis of Ligands H₂L^{1−5}. The salophen ligands $H_2L^{1−4}$ were prepared in a fair yield by the condensation of *o*-phenylenediamine with the corresponding aldehydes (salicylaldehyde (H_2L^1), *o*-vanillin (H_2L^2), 5-bromosalicylaldehyde (H_2L^3), and 2-hydroxy-1-naphthaldehyde (H_2L^4)) in a 1:2 ratio in ethanol by a adapting a reported procedure.[43] The resulting dark orange compounds were filtered and then washed with ethanol and finally dried over fused $CaCl_2$. H_2L^5 was synthesized by condensing 1,2-diaminopropane with *o*-vanillin as reported in the literature.[44] Elemental analysis results and NMR (^1H and ^{13}C) and IR data for all of these confirmed their preparation. The ^1H NMR data of $H_2L^{1−5}$ have been included in Table S1.

H₂L^1. Yield: 65%. Anal. Calcd for $C_{20}H_{16}N_2O_2$: C, 75.93; H, 5.10; N, 8.86. Found: C, 75.92; H, 5.17; N, 8.81. IR (KBr pellet, cm^{-1}): 3320 ν(O−H), 1623 ν(C=N). ^{13}C NMR (100 MHz, DMSO-d_6): δ (ppm) = 164.51, 160.84, 142.72, 133.91, 132.91, 128.28, 120.21, 119.94, 119.55, 117.13.

H₂L^2. Yield: 67%. Anal. Calcd for $C_{22}H_{20}N_2O_4$: C, 70.20; H, 5.36; N, 7.44. Found: C, 70.23; H, 5.34; N, 7.41. IR (KBr pellet, cm^{-1}): 3484 ν(O−H), 1611 ν(C=N). ^{13}C NMR (100 MHz, DMSO-d_6): δ (ppm) = 161.33, 157.54, 151.59, 146.37, 129.37, 127.65, 122.48, 121.67, 120.86, 118.19, 79.57.

Table 1. Crystal Data and Refinement Data of Complexes 1, 2, 4, and 5

	1	2	4	5
formula	$C_{26}H_{18}Mo_2N_4O_4$	$C_{28}H_{22}Mo_2N_4O_6$	$C_{34}H_{22}Mo_2N_4O_4$	$C_{19}H_{20}MoN_2O_6$
M	642.32	702.38	742.44	468.31
cryst sym	triclinic	triclinic	monoclinic	triclinic
space group	$P\bar{1}$	$P\bar{1}$	$P2_1/n$	$P\bar{1}$
a (Å)	8.5389(13)	9.4562(5)	8.9152(3)	11.9576(11)
b (Å)	10.4521(14)	9.6471(5)	17.7572(6)	12.8243(13)
c (Å)	13.565(2)	14.4626(7)	17.7893(6)	13.8984(14)
α (deg)	88.732(9)	79.619(2)	90	76.348(8)
β (deg)	80.213(9)	79.536(3)	104.473(3)	77.430(8)
γ (deg)	70.999(9)	88.060(2)	90	78.140(8)
V (Å^3)	1127.3(3)	1276.17(11)	2726.84(16)	1994.6 (3)
Z	2	2	4	4
D_{calc} (g cm^{-3})	1.892	1.828	1.808	1.556
μ(Mo Kα) (mm^{-1})	1.156	1.036	7.948	0.695
$F(000)$	636	700	1480	952
max/min transm	0.988/0.893	0.9597/0.9125	0.933/0.793	0.933/0.793
θ (max) (deg)	26.77	28.36	73.97	25.00
temp (K)	110	100	100	200
reflns collected	10634	54801	8414	9605
R^a [$I > 2\sigma(I)$]	0.0538	0.0250	0.0487	0.0513
$R_w{}^b$ [all data]	0.1103	0.0629	0.1336	0.1035
S [goodness of fit]	0.974	1.062	1.040	0.826
max/min res (e Å^{-3})	0.914/−0.895	0.658/−0.670	1.549/−0.662	0.483/−0.692

$^a R = \dfrac{\sum \|F_o| - |F_c\|}{\sum (|F_o|)}$. $^b R_w = \sqrt{\sum [w(F_o{}^2 - F_c{}^2)^2]/\sum [w(F_o{}^2)^2]}$.

H₂L³. Yield: 62%. Anal. Calcd for $C_{20}H_{14}Br_2N_2O_2$: C, 50.66; H, 2.98; N, 5.91. Found: C, 50.62; H, 2.95; N, 5.90. IR (KBr pellet, cm^{-1}): 3480 ν(O−H), 1611 ν(C=N). ^{13}C NMR (100 MHz, DMSO-d_6): δ (ppm) = 162.67, 159.92, 142.45, 136.15, 134.23, 128.64, 121.88, 120.11, 119.63, 110.36.

H₂L⁴. Yield: 68%. Anal. Calcd for $C_{28}H_{20}N_2O_2$: C, 80.75; H, 4.84; N, 6.73. Found: C, 80.71; H, 4.82; N, 6.70. IR (KBr pellet, cm^{-1}): 3488 ν(O−H), 1619 ν(C=N). ^{13}C NMR (100 MHz, DMSO-d_6): δ (ppm) = 169.06, 157.82, 138.93, 137.27, 133.46, 129.46, 128.66, 127.89, 127.34, 124.11, 121.95, 121.06, 120.17, 109.70.

H₂L⁵. Yield: 64%. Anal. Calcd for $C_{19}H_{22}N_2O_4$: C, 66.65; H, 6.48; N, 8.18. Found: C, 66.63; H, 6.45; N, 8.12. IR (KBr pellet, cm^{-1}): 3692 ν(O−H), 1627 ν(C=N). ^{13}C NMR (100 MHz, DMSO-d_6): δ (ppm) = 167.54, 165.68, 152.01, 151.66, 148.43, 148.37, 123.62, 123.56, 118.70, 118.61, 118.33, 118.20, 115.17, 115.04, 64.44, 63.84, 56.14, 56.02, 20.33.

Synthesis of Complexes [Mo₂ᵛO₂L′₂¹⁻⁴] (1−4). [MoO₂(acac)₂] (1 mmol) was added to a refluxing solution of the appropriate ligand H₂L¹⁻⁴ (1 mmol) in 20 mL of ethanol; the color initially changed to pale blue and then to dark red. The change of color from pale blue to red was very fast for **1−3**, while for **4** the color remained blue until 15 min. The reflux was continued for 3 h and filtered. A dark red residue was obtained. Red crystals of **1**, **2**, and **4** were obtained by recrystallizing the residue in DMSO. The X-ray quality crystals obtained were filtered and washed with ethanol. Due to the poor quality of the crystals of **3**, its X-ray structure could not be solved. Elemental analysis results and IR, NMR (^{1}H, ^{13}C), UV−vis, and ESI-MS data for all of the complexes verified their preparation. The ^{1}H NMR data of [Mo₂ᵛO₂L′₂¹⁻⁴] (**1−4**) and [MoᵛᴵO₂L⁵] (**5**) have been included in Table S1.

[Mo₂ᵛO₂L′₂¹] (1). Yield: 34%. Anal. Calcd for $C_{26}H_{18}Mo_2N_4O_4$: C, 48.62; H, 2.82; N, 8.72. Found: C, 48.60; H, 2.81; N, 8.73. Main IR peaks (KBr pellet, cm^{-1}): 1601 ν(C=N), 951, 855 ν(Mo=O). UV−vis (DMSO): λ_{max}, nm (ε, dm^3 mol^{-1} cm^{-1}): 465 (2824), 368 (6422), 320 (13313), 290 (18595). ^{13}C NMR (100 MHz, DMSO-d_6): δ (ppm) = 177.30, 172.51, 161.61, 147.74, 142.03, 137.44, 136.87, 133.79, 122.48, 121.97, 116.76, 112.23, 111.97. ESI-MS: m/z 642.15 [M]$^+$.

[Mo₂ᵛO₂L′₂²] (2). Yield: 32%. Anal. Calcd for $C_{28}H_{22}Mo_2N_4O_6$: C, 47.88; H, 3.16; N, 7.98. Found: C, 47.84; H, 3.12; N, 7.94. IR (KBr pellet, cm^{-1}): 1598 ν(C=N), 946, 912 ν(Mo=O). UV−vis (DMSO): λ_{max}, nm (ε, dm^3 mol^{-1} cm^{-1}): 483 (11914), 395 (20699), 328 (46037), 275 (52678). ^{13}C NMR (100 MHz, DMSO-d_6): δ (ppm) = 155.28, 153.70, 151.87, 148.94, 134.32, 129.02, 126.17, 122.34, 118.89, 118.21, 116.53, 115.70, 115.57, 55.74. ESI-MS: m/z 702.16 [M]$^+$.

[Mo₂ᵛO₂L′₂³] (3). Yield: 35%. Anal. Calcd for $C_{26}H_{16}Br_2Mo_2N_4O_4$: C, 39.03; H, 2.02; N, 7.00. Found: C, 39.01; H, 2.00; N, 7.02. IR (KBr pellet, cm^{-1}): 1597 ν(C=N), 911, 883 ν(Mo=O). UV−vis (DMSO): λ_{max}, nm (ε, dm^3 mol^{-1} cm^{-1}): 484 (9759), 383 (17993), 276 (57553). ^{13}C NMR (100 MHz, DMSO-d_6): δ (ppm) = 162.90, 154.61, 152.45, 137.33, 136.86, 134.63, 129.94, 124.63, 121.76, 119.02, 116.30, 116.22, 110.88. ESI-MS: m/z 800.64 [(M − H) $^+$].

[Mo₂ᵛO₂L′₂⁴] (4). Yield: 26%. Anal. Calcd for $C_{34}H_{22}Mo_2N_4O_4$: C, 55.00; H, 2.99; N, 7.55. Found: C, 55.02; H, 2.94; N, 7.52. IR (KBr pellet, cm^{-1}): 1565 ν(C=N), 937, 912 ν(Mo=O). UV−vis (DMSO): λ_{max}, nm (ε, dm^3 mol^{-1} cm^{-1}): 486 (15710), 397 (17833), 349 (30945), 279 (55015). ^{13}C NMR (100 MHz, DMSO-d_6): δ (ppm) = 193.30, 169.13, 157.79, 138.91, 138.86, 137.30, 133.46, 129.47, 129.30, 128.66, 127.89, 127.32, 124.72, 124.11, 121.98, 121.07, 109.68. ESI-MS: m/z 742.28 [M]$^+$.

Synthesis of the Intermediate Species [MoᵛO(HL′⁴)(OEt)] (I$_d$⁴). [MoO₂(acac)₂] (1 mmol) was added to a refluxing solution of H₂L⁴ (1 mmol) in ethanol. The solution turned pale blue, the reaction was stopped after 15 min when the solution was still blue, and the mixture was filtered. Blue residue of I$_d$⁴ was obtained. Elemental analysis results and IR, UV−vis, EPR, ESI-MS, and cyclic voltammetry data for the complex verified its preparation. The corresponding intermediates [MoᵛO(HL′¹⁻³)(OEt)] (I$_d$¹⁻³) could not be isolated because of their very fast conversion into the dimeric species [Mo₂ᵛO₂L′₂¹⁻³] (**1−3**).

In an alternative strategy, when [MoO₂(acac)₂] (1 mmol) was added to a refluxing solution of H₂L⁴ (1 mmol) in ethanol in the presence of few drops of water, the solution remained blue for 30 min and blue crystalline residue of I$_d$⁴ was now obtained in a higher yield.

[MoᵛO(HL′⁴)(OEt)] (I$_d$⁴). Yield: 15%. Anal. Calcd for $C_{19}H_{17}MoN_2O_3$: C, 54.69; H, 4.11; N, 6.71. Found: C, 54.64; H,

4.10; N, 6.73. IR (KBr pellet, cm^{-1}): 3062 ν(−NH), 1568 ν(−C=N), 949 ν(Mo=O). UV−vis (DMSO): λ_{max}, nm (ε, dm^3 mol^{-1} cm^{-1}): 607 (4692), 562 (2917), 519 (1466), 323 (14222), 274(46436). ESI MS: m/z 421.64 [(M + 2H)$^+$].

Synthesis of [Mo^{VI}O$_2$L^5] (5). [MoO$_2$(acac)$_2$] (1 mmol) was added to a refluxing solution of H$_2$L^5 (1 mmol) in 20 mL of ethanol; the color changed to orange. The solution was refluxed for 3 h. Dark orange crystalline residue of **5** was obtained on filtering the solution. Some of the crystals were of good quality and were used directly for X-ray analysis. Elemental analysis results and IR, NMR (^{1}H, ^{13}C), UV−vis, and ESI-MS data for the complex verified its preparation.

[Mo^{VI}O$_2$L^5] (5). Yield: 42%. Anal. Calcd for C$_{19}$H$_{20}$MoN$_2$O$_6$: C, 48.73; H, 4.30; N, 5.98. Found: C, 48.71; H, 4.29; N, 5.94. IR (KBr pellet, cm^{-1}): 1607 ν(C=N), 907, 874 ν(Mo=O). UV−vis (DMSO): λ_{max}, nm (ε, dm^3 mol^{-1} cm^{-1}): 438 (1871), 323 (7254), 278 (12155). ^{13}C NMR (100 MHz, DMSO-d_6): δ (ppm) = 164.21, 159.45, 150.85, 150.71, 149.61, 148.93, 132.08, 129.14, 126.65, 126.29, 124.98, 124.47, 123.62, 123.55, 122.39, 121.74, 121.67, 121.60, 121.29, 118.72, 118.64, 118.34, 118.20, 117.68, 117.24, 116.91, 116.78, 116.54, 115.18, 115.05, 67.85, 64.51, 63.90, 62.64, 38.51, 30.24, 28.82, 22.87. ESI-MS: m/z 468.12 [M]$^+$.

Crystallography. Clear inclusion free single crystals of **1, 2, 4,** and **5** suitable for X-ray diffraction studies were mounted on loops with oil. Crystallographic data and details of refinement are collected in Table 1. The compounds **1, 2,** and **5** crystallize in the triclinic space group $P\bar{1}$, and **4** crystallizes in monoclinic space group $P2_1/n$. The unit cell parameters and the intensity data were recorded for complexes **1** and **2** on a Bruker APEX II employing graphite monochromated Mo Kα radiation (λ = 0.71073 Å) at ∼110 K and ∼100 K respectively. The data for complex **4** were collected on SuperNova AS2 Data Collections using high intensity of SuperNova microfocus Cu Kα source (λ = 1.54184 Å) and a highly sensitive Atlas CCD detector at ∼100 K. Single crystals of complex **5** were mounted on a Stoe IPDS 2 diffractometer equipped with an Oxford Cryosystem open flow cryostat employing a graphite monochromated Mo Kα radiation (λ = 0.71073 Å) at ∼200 K. The intensity data were corrected for Lorentz, polarization, and absorption effects. The data was integrated and scaled using SAINT, SADABS within the APEX2 software package by Bruker.[45a] The structures were solved using the SHELXS97[45b] and refined using SHELXL97[46] computer programs. Hydrogen atoms were set in geometrically idealized positions and constrained to ride on their parent atoms with C−H distances in the range 0.95−1.00 Å. Isotropic thermal parameters U_{eq} were defined such that they were 1.2U_{eq} of their parent atom U_{eq} for CH's and 1.5U_{eq} of their parent atom U_{eq} in the case of methyl groups. All the non-hydrogen atoms were refined anisotropically by full-matrix least-squares.

DNA Binding Experiments. *Using Absorption Spectroscopy.* The binding of the dimeric oxidomolybdenum(V) and monomeric dioxidomolybdenum(VI) complexes to calf thymus DNA (CT-DNA) was examined as previously described.[38c−g] Briefly, the UV−vis titration experiments were carried out with variable CT-DNA concentrations (0−50 μM) against a fixed concentration of molybdenum complex (25 μM) in 10 mM Tris−HCl buffer (pH 8.0) containing 1% DMF using a Lambda 35 PerkinElmer (USA) spectrophotometer. The binding of ligands to CT-DNA was also studied. To do this the concentration of ligand was fixed at 25 μM and was titrated with variable DNA concentration (0−250 μM) in 10 mM Tris−HCl buffer (pH 8.0) containing 1% DMF. The data obtained from the titration experiments were then fit to the following equation to obtain binding constant K_b:[38c−g]

$$\frac{[DNA]}{\varepsilon_a - \varepsilon_f} = \frac{[DNA]}{\varepsilon_b - \varepsilon_f} + \frac{1}{K_b(\varepsilon_b - \varepsilon_f)} \qquad (1)$$

where [DNA] is the concentration of DNA base pairs, ε_a, ε_f, and ε_b correspond to apparent extinction coefficients for the complex, i.e., Abs/[complex] in the presence of DNA, in the absence of DNA, and fully bound DNA, respectively. A plot of [DNA]/($\varepsilon_a - \varepsilon_f$) vs [DNA] resulted in a slope and intercept equal to 1/($\varepsilon_b - \varepsilon_f$) and 1/$K_b(\varepsilon_b - \varepsilon_f$

ε_f), respectively; K_b is determined from the ratio of the slope to the intercept.

Using Thermal Denaturation Technique. Thermal denaturation studies of CT-DNA (100 μM) in the absence and presence of molybdenum complexes (25 μM) were carried out by monitoring the absorbance at 260 nm in the temperature range of 30−90 °C in 10 mM Tris−HCl buffer (pH 8.0) containing 1% DMF. The ramp rate for each of the experiments was 0.5 °C/min. All the experiments were carried out in absorbance mode using a Chirascan CD spectropolarimeter (Applied Photophysics, U.K.) equipped with a Peltier temperature controller. The melting temperature (T_m) was determined from the derivative plot (dA_{260}/dT vs T) of the melting profile.[47a]

Using Circular Dichroism Spectroscopy. Circular dichroism (CD) spectroscopy was studied using a Chirascan CD spectropolarimeter (Applied Photophysics, U.K.) at 25 °C. CD spectra of CT-DNA (100 μM) in the absence and presence of molybdenum complexes (25 μM) were obtained in the wavelength range of 240−400 nm in 10 mM Tris−HCl buffer (pH 8.0) containing 1% DMF using quartz cell with 10 mm path length.[38c−g]

Fluorescence Experiments. The fluorescence spectra of the complexes **1−5** (100 μM) as well as ligands (100 μM) in 10 mM Tris−HCl buffer (pH 8.0) containing 1% DMF at 25 °C were recorded using a spectrofluorimeter using Fluoromax 4P (Horiba Jobin Mayer, USA).
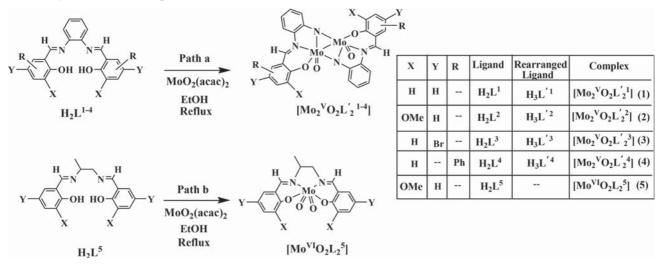
DNA Cleavage Experiments. For all experiments, 300 ng of supercoiled (SC) pUC19 DNA was used, in the presence of 50 mM Tris−HCl buffer (pH 8.0) containing 1% DMF.

Chemically Induced DNA Cleavage. For chemical nuclease studies, the cleavage experiments were executed in the dark employing hydrogen peroxide (0.5 mM) as the oxidizing agent in the absence and presence of the molybdenum complexes (1−100 μM). The incubation temperature was fixed at 37 °C for 3 h and analyzed for DNA cleaved products by agarose gel electrophoresis.
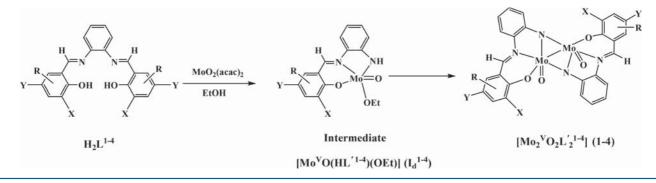
Photoinduced DNA Cleavage. The photoinduced DNA cleavage studies were carried out according to literature procedures.[38c−g] Briefly, the photolytic DNA cleavage experiments were performed on supercoiled (SC) pUC19 DNA (300 ng) with **1−5** (1−100 μM) in 50 mM Tris HCl buffer (pH 8.0) containing 1% DMF. The extent of DNA cleavage was calculated from the intensities of the bands using the UVP Gel Documentation System (Gel Doc It^2). The error observed in determining the band intensities was between 3−6%. Four different additives (two singlet oxygen quenchers (sodium azide and L-histidine) and two hydroxyl radical quenchers (KI and D-mannitol)) were used to discern the mechanistic aspect behind the DNA cleavage. These additives were added to the reaction mixture before the addition of the complex. The concentration of each of the additives was 0.5 mM.

Cytotoxicity Studies. *MTT Assay.* MCF-7 cells were cultured in DMEM having 10% FBS and penicillin (100 U/mL) and streptomycin (100 μg/mL) in a humidified 5% CO$_2$ incubator at a temperature of 37 °C. HCT 15 cells were cultured in RPMI 1640 containing 10% FBS and penicillin (100 U/mL) and streptomycin (100 μg/mL) in a humidified 5% CO$_2$ incubator at 37 °C. HaCaT cells were cultured in DMEM having 10% FBS and penicillin (100 U/mL) and streptomycin (100 μg/mL) in a humidified 5% CO$_2$ incubator at a temperature of 37 °C. The cytotoxicity was assayed by determining the viability of MCF-7, HCT-15, and HaCaT cells after treatment by **1−5** through MTT assay. Briefly, the cells (10^5 cells/well) were seeded in 96-well plates in DMEM containing 10% FBS. After cells reached confluency, treatment was given with varying concentrations (5 μM, 10 μM, 25 μM, and 50 μM) of the molybdenum complexes. The complexes were dissolved in DMSO, and working solutions were prepared by diluting the stock of a 5 mM concentration of each compound with plain DMEM. Final working concentration of DMSO in assay was less than 2%. Untreated cells were taken as 100% survival. After the treatment, medium was removed and cells were incubated with MTT (5 mg/mL) for 4 h. The crystals formed were dissolved in DMSO, and absorbance was read at 570 nm. IC$_{50}$ was calculated for each compound by treating the cells for 48 h.

Scheme 1. Synthesis of Dimeric Oxidomolybdenum(V) Complexes $[Mo_2^VO_2L'_2^{1-4}]$ (1−4) and Monomeric Dioxidomolybdenum(VI) Complex $[Mo^{VI}O_2L^5]$ (5)

X	Y	R	Ligand	Rearranged Ligand	Complex
H	H	--	H_2L^1	$H_3L'^1$	$[Mo_2^VO_2L'_2^1]$ (1)
OMe	H	--	H_2L^2	$H_3L'^2$	$[Mo_2^VO_2L'_2^2]$ (2)
H	Br	--	H_2L^3	$H_3L'^3$	$[Mo_2^VO_2L'_2^3]$ (3)
H	--	Ph	H_2L^4	$H_3L'^4$	$[Mo_2^VO_2L'_2^4]$ (4)
OMe	H	--	H_2L^5	--	$[Mo^{VI}O_2L_2^5]$ (5)

Scheme 2. Schematic Pathway for the Formation of $[Mo_2^VO_2L'_2^{1-4}]$ (1−4) via the Intermediate $[Mo^VO(HL'^{1-4})(OEt)]$ (I_d^{1-4})

Propidium Iodide Staining. Propidium iodide (or PI) is an intercalating agent which has the fluorescence excitation maximum is 535 nm, and the emission maximum is 617 nm.[47b] PI staining was carried out to visualize the morphology of the nuclei after the treatment with 1−5. The MCF-7 (human breast cancer cells), HCT-15 (colon cancer cells), and HaCaT (immortalized human keratinocytes) cells were grown in the 96-well plate. After reaching approximately 90% confluency, the cells were treated with varying concentrations (5, 10, 25, 50 μM) of 1−5 and were incubated for 48 h. Cells were observed under an inverted fluorescence microscope after treatment to check for morphological changes, during cell death. Then the cells were washed twice with PBS (pH 7.4) and fixed after incubation for 15 min with 3.7% of formaldehyde. The cells were further washed twice with PBS and treated with 0.2% Triton X-100 in PBS for 30 s. Again, the washing was repeated with PBS and PI solution (10 μg/mL) was added, and the sample was kept in the dark for 15 min. At the end, the cells were further washed with PBS and imaged under a fluorescence microscope (FLoid, Life Technologies and Olympus IX 70).

RESULTS AND DISCUSSION

Synthesis. Scheme 1 portrays the synthesis of four dimeric oxidomolybdenum(V) complexes $[Mo_2^VO_2L'_2^{1-4}]$ (1−4), where L'^{1-4} indicates the rearranged form of the ligands H_2L^{1-4}, and a monomeric dioxidomolybdenum(VI) complex (5), via two different reaction pathways (path a and path b), from salen type ligands (H_2L^{1-5}).
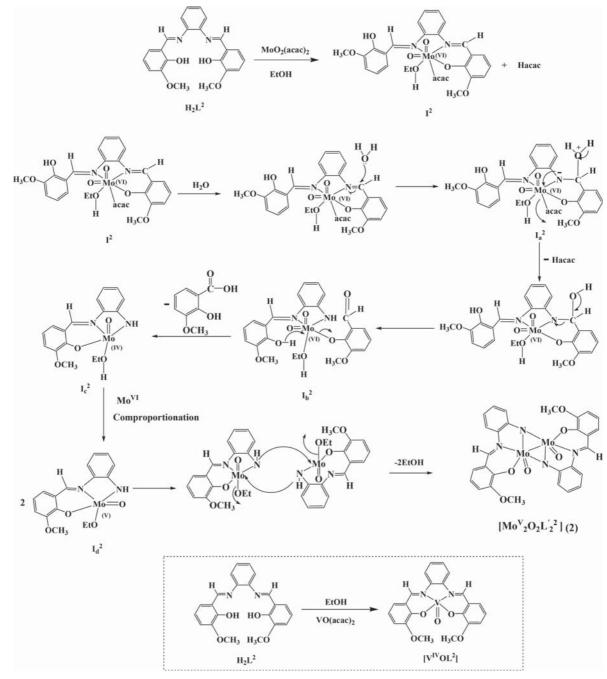
When the ligands were subjected to reflux in the presence of $MoO_2(acac)_2$, H_2L^{1-4} (which contained the aromatic diimine) followed the reaction path a (Scheme 1) which involved a

Mo(V) intermediate, $[Mo^VO(HL'^{1-4})(OEt)]$ (I_d^{1-4}), and finally dimeric bis-μ-imido bridged oxidomolybdenum(V) complexes $[Mo_2^VO_2L'_2^{1-4}]$ (1−4) were formed, containing rearranged ligands $H_3L'^{1-4}$ furnished by Mo assisted hydrolysis and −C≡N bond cleavage (Scheme 2). One of the intermediates, I_d^4, has been isolated in the solid state and characterized by UV−vis, IR, EPR, ESI-MS, and cyclic voltammetry.

The detailed mechanism of the formation of $[Mo_2^VO_2L'_2^{1-4}]$ (1−4) is shown in Scheme 3, taking H_2L^2 as a representative among the four ligands, which illustrates that at first a dioxidomolybdenum(VI) species $[Mo^{VI}O_2(HL^2)(acac)(EtOH)]$ (I^2) is formed, and then a molybdenum assisted hydrolysis of one of the coordinated −C≡N bonds of the salophen ligand leads to the formation of I_b^2, via the formation of I_a^2 and release of Hacac.[47c] The pendant phenolic OH then coordinates to the metal center, and removal of the aldehyde (o-vanillin) as an acid (o-vanillic acid)[47d] takes place in lieu of the reduction of Mo(VI) species (I_b^2) to Mo(IV) species (I_c^2). The Mo(IV) species, I_c^2, then undergoes a fast comproportionation[47e] reaction with a Mo(VI) species present in the reaction medium to form a Mo(V) intermediate I_d^2. Finally deprotonation and dimerization of I_d^2 occurs with the loss of ethanol, and μ-imido bridges between two molybdenum fractions are furnished to yield $[Mo_2^VO_2L'_2^2]$ (2).

In the above reaction, water plays a significant role. In fact, when the same reaction is carried out in the presence of few drops of water, it has been found that the yield of 2 increases

5

Scheme 3. Proposed Mechanistic Pathway of Formation of Dimeric Oxidomolybdenum(V) Complex [Mo$_2^V$O$_2$L$'_2^2$] (2) and the Corresponding Oxidovanadium(IV) Complex, [V^{IV}OL^2][41a,b]

significantly. There are reports of vanadium complexes of similar ligands where such hydrolysis and −C═N bon cleavage of salophens did not take place in the presence of VO(acac)$_2$ (Scheme 3).[41a,b] It has also been found in the literature that, in the presence of several other transition metals (Ti,[41c] Cr,[41d] Mn,[41e] Fe,[41f] Co,[41g] Ni,[41h] Cu,[41i] Zn,[41j] W,[35c] Os,[41k] and Pt[41l]), −C═N bond cleavage of salophens does not take place, which proves that the hydrolysis and −C═N bond cleavage of salophens in complex 1−4 is molybdenum assisted. X-ray crystallography (discussed later) revealed the presence of a localized metal−metal single bond between the two molybdenum(V) centers of all the oxidomolybdenum(V) complexes [Mo$_2^V$O$_2$L$'_2^{1-4}$] (1−4). The formation of the monomeric dioxidomolybdenum(VI) complex [Mo^{VI}O$_2$L^5]

(5) took place via path b (Scheme 1), where no such hydrolysis and −C═N bond cleavage of H$_2$L^5 occurred in the presence of MoO$_2$(acac)$_2$ owing to the fact that, during the −C═N bond cleavage, the corresponding intermediate, [Mo^{VI}O$_2$(HL^5)(EtOH)(acac)(H$_2$O)] (I$_a^5$), would not get any resonance stabilization due to the absence of aromatic backbone in the ligand environment, which is available in the case of I$_a^{1-4}$. 1−5 were completely soluble in DMF and DMSO and partly soluble in CH$_3$CN, CH$_2$Cl$_2$, and H$_2$O. The complexes were stable in both solution and solid phases. The solution phase stability of the complexes for the biological assays was confirmed by electronic absorption and NMR studies (Figure S1A−C). From the magnetic susceptibility and molar conductivity data, it could be concluded that all the
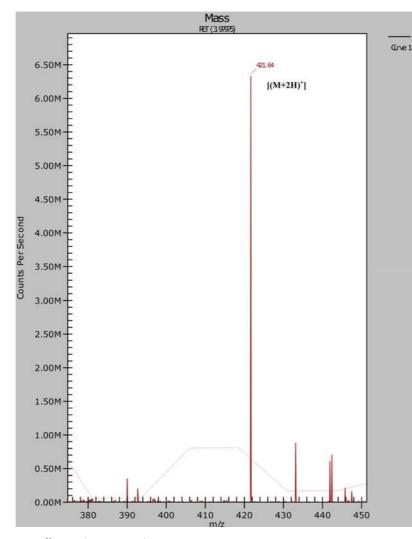
Figure 1. ESI-MS spectrum of $[Mo^VO(HL'^4)(OEt)]$ (I_d^4).

complexes (**1**−**5**) are diamagnetic and electrically nonconducting in solution. The oxidomolybdenum(V) complexes (**1**−**4**) are silent in electron paramagnetic resonance (EPR) spectroscopy, which may be attributed to the antiferromagnetic coupling[48a] of electron spins of the two $4d^1$ Mo(V) ions and the formation of an Mo–Mo bond.[1,3i,48b,c]

IR Spectroscopy. Selected IR data of all the ligands (H_2L^{1-5}) and the complexes **1**−**5** are given in the Experimental Section. The ligands showed a minimum intensity IR band in the range of 3320−3692 cm^{-1} due to $\nu(OH)$ stretching.[43] Distinct bands within the range of 1611−1627 cm^{-1} due to $\nu(C=N)$ of azomethine groups of the salen type ligands[32,43] (H_2L^{1-5}) were noticed. In the complexes (**1**−**5**), the $\nu(C=N)$ stretching was shifted to lower frequencies (1565−1607 cm^{-1}), which might be attributable to the lower C=N bond order due to the coordination to the metal atom.[33] In addition, the complexes **1**−**5** display a pair of sharp strong peaks in the range 855−951 cm^{-1} due to $\nu(M=O)$ stretch.[49a−c] The intermediate $[Mo^VO(HL'^4)(OEt)]$ (I_d^4), which has been isolated, showed a strong oxido peak at 949 cm^{-1} due to a single $\nu(M=O)$ stretch.[49a−c] Absorption at 3062 cm^{-1} is observed which can be attributed to the $\nu(NH)$ stretching;[38d] the peak at 1568 cm^{-1} is due to the −C=N stretching[38a] of the imine bond of the salophen ligand. Representative spectra of complex **4** and its corresponding intermediate I_d^4 are given in Figure S2.

UV−Vis Spectroscopy. The electronic absorption spectra of the complexes **1**−**5** and I_d^4 were recorded in DMSO. The spectral data are summarized in the Experimental Section. The spectra of **1**−**5** display a shoulder in the 438−486 and two strong absorptions in the 275−397 nm range which are assignable to LMCT and intraligand transitions, respectively.[49a−c] The absorption spectrum of $[Mo^VO(HL'^4)(OEt)]$ (I_d^4) exhibits peaks at 607, 562, 519, 323, and 274 nm. The band at 323 and 274 nm is attributed to the intraligand charge transfer band; the bands at 562 and 519 nm are assigned as LMCT bands.[49a−c] The low energy transition band at 607 nm is located in the d−d transition region as evidenced from previous reports of oxidomolybdenum complexes.[49c−e] However, the unusually high intensity of this band (ε_{max}, 4692 dm^3 mol^{-1} cm^{-1}), which is too high for a pure d−d transition,[38a] and analogy with other molybdenum(V) complexes[49f] suggest that this transition may be due to the presence of a mixture of LMCT and d−d transitions. The representative spectra of complex **4** and I_d^4 are given in Figure S3.

NMR Spectroscopy. ^1H and ^{13}C NMR of all the compounds were recorded in DMSO-d_6. The ^1H NMR data are collected in Table S1, and the ^{13}C NMR data are given in the Experimental Section. The coordinating modes of H_2L^{1-5} were confirmed by comparing their ^1H NMR spectral patterns with those of the corresponding complexes. The representative

^{1}H NMR spectra of H_2L^2, $[Mo_2^VO_2L'_2^2]$ (**2**), and $[Mo_2^VO_2L'_2^3]$ (**3**) are given in Figures S4a, S4b, and S5, respectively. The ^{1}H NMR spectrum of the free ligands exhibits resonance in the range $\delta = 12.96-15.13$ ppm due to phenolic OH and at $\delta = 8.52-9.68$ ppm due to the azomethine $-CH$ protons, respectively.[50a] The signals for the aromatic protons from ligands are observed in the expected region $\delta = 6.75-8.54$ ppm. Singlets for the $-OCH_3$ protons of H_2L^2 and H_2L^5 are observed at around 3.74 ppm. The aliphatic protons of H_2L^5 appear as two doublets at 3.73 and 1.31 ppm for $-CH_2$ and $-CH_3$ respectively, and a multiplet is observed at 3.77 ppm for $-CH$ proton.[50] In the NMR spectra of complexes, the peak for the aromatic $-OH$ proton was not observed due to the deprotonation of phenolic group. The NMR spectrum of complex **5** exhibits double the number of protons due to the presence of two entities in one unit.

In the ^{13}C NMR spectra of the ligands H_2L^{1-5}, spectral signals for the aromatic carbons are found in the range of $\delta = 109.70-169.06$ ppm.[50b] The signals for the aliphatic carbons of H_2L^5 are found in the range $\delta = 20.33-64.44$ ppm, and the signal for $-OCH_3$ carbon of H_2L^2 appears at 79.57 ppm, while in the ^{13}C NMR spectra of complexes **1–5**, signals for the aromatic carbons are found in the downfield region in the range $\delta = 109.68-193.30$ ppm.[50] The signals for $-OCH_3$ carbon and aliphatic carbons of the complexes **2** and **5** appear in the range $\delta = 22.87-67.85$ ppm. Figure S6 shows the ^{13}C NMR spectrum of **3**.

ESI-MS. ESI-MS spectra of **1–5** and I_d^4 have been recorded in DMSO. The characteristic molecular ion peaks for **1–5** appear at 642.15 $[M]^+$, 702.16 $[M]^+$, 800.64 $[(M - H)^+]$, 742.28 $[M]^+$, and 468.12 $[M]^+$, respectively, while the molecular ion peak for I_d^4 appears at 421.64 $[(M + 2H)^+]$. The representative ESI-MS spectra of I_d^4 and **3** are given in Figure 1 and Figure S7, respectively.

EPR Spectroscopy of the Intermediate Monomeric Mo(V) Compound $[Mo^VO(HL'^4)(OEt)]$ (I_d^4). EPR spectra were recorded at room temperature (298 K) as a function of the time on I_d^4 (Schemes 2 and 3), dissolved in a degassed DMSO solution. These are shown in Figure 2. The spectra
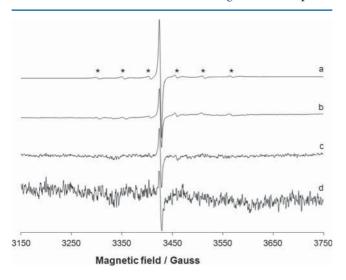

Figure 2. EPR spectra recorded at 298 K as a function of the time on I_d^4 dissolved in a degassed DMSO solution: (a) $t = 7$ min; (b) $t = 14$ min; (c) $t = 20$ min; (d) $t = 26$ min. With the asterisks the six hyperfine lines due to the coupling between the unpaired electron with ^{95}Mo and ^{97}Mo nuclei are indicated.

consist of a strong central signal due to the coupling between an unpaired electron with the nonmagnetic nuclei ^{92}Mo, ^{94}Mo, ^{96}Mo, ^{98}Mo, and ^{100}Mo ($I = 0$; total natural abundance 74.5%) and six hyperfine lines due to the coupling with ^{95}Mo and ^{97}Mo nuclei ($I = 5/2$; total abundance 25.5%), indicated by the asterisks in Figure 2. No signals below 3250 G and above 3650 G were revealed. These features demonstrate that the oxidation state of Mo is +V with only one electron in the 4d orbitals (configuration $4d^1$).[51a] The examination of the EPR spectra indicates the presence of only one species in the organic solution (I_d^4), characterized by $g_{iso} = 1.955$ and $A_{iso} = 40.4 \times 10^{-4}$ cm^{-1}. These spin Hamiltonian parameters are consistent with a $Mo(N_2{}^{\wedge}O_2)$ equatorial coordination mode[51b] and fall in the range expected by the correlation between g_{iso} and A_{iso} proposed some years ago by Enemark and co-workers.[51c]

As it can be observed, the spectral signals decrease significantly in the time range 0–26 min (at $t = 26$ min, only the central absorption is detected and the signal-to-noise ratio is very low) and disappear completely for time longer than 30 min, suggesting a probable antiferromagnetic[48a] coupling between the unpaired electrons of the Mo(V) centers in the bis-μ-imido bridged oxidomolybdenum(V) complex (**4**) formed upon the dimerization of two intermediate I_d^4 species (Scheme 3).

Electrochemical Properties. Electrochemical properties of the complexes **1–5** have been studied by cyclic voltammetry in DMF solution, and that of I_d^4 has been studied in DMSO (0.1 M TBAP). The CV traces of all the binuclear oxidomolybdenum(V) complexes $[Mo_2^VO_2L'_2^{1-4}]$ (**1–4**) are of similar pattern, and a representative voltammogram of $[Mo_2^VO_2L'_2^4]$ (**4**) is discussed herein. The redox potentials of all the complexes are summarized in Table 2. It is observed that
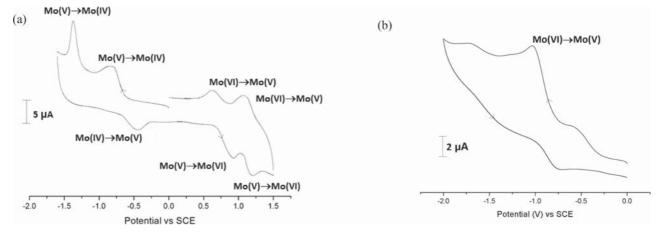
Table 2. Cyclic Voltammetric Results for 1–5 and (I_d^4) at 298 K[a]

complex	$E^c_{1/2}$ (V), E_{pc} (V)	ΔE_p (mV)	$E^a_{1/2}$ (V)	ΔE_p (mV)
$[Mo_2^VO_2L'_2^1]$ (**1**)	−0.61, −1.36	372	0.76, 1.14	300, 130
$[Mo_2^VO_2L'_2^2]$ (**2**)	−0.63, −1.33	340	0.75, 1.11	300, 120
$[Mo_2^VO_2L'_2^3]$ (**3**)	−0.62, −1.35	365	0.76, 1.13	310, 140
$[Mo_2^VO_2L'_2^4]$ (**4**)	−0.63, −1.37	370	0.78, 1.14	310, 110
$[Mo^{VI}O_2L^5]$ (**5**)	−0.89, −1.69	270		
$[Mo^VO(HL'^4)(OEt)]$ (I_d^4)	−0.91	286		

[a]Solvent: DMF for **1–5** and DMSO for I_d^4. Pt working and auxiliary electrodes and SCE as reference electrode and TBAP as supporting electrolyte. Scan rate: 50 mV/s. $E_{1/2} = (E_{pa} + E_{pc})/2$, where E_{pa} and E_{pc} are anodic and cathodic peak potentials vs SCE, respectively. $\Delta E_p = E_{pa} - E_{pc}$.

4 exhibits a single electron quasi-reversible reductive response at $E_{1/2}$ value of −0.63 V and an irreversible reductive response at −1.37 V (Figure 3a) which can be assigned to the reduction of $Mo(V) \rightarrow Mo(IV)$ of the two corresponding molybdenum centers.[52] Further, two single electron quasi-reversible oxidative responses at $E_{1/2}$ value of 0.78 and 1.14 V can be attributed to the oxidation of $Mo(V) \rightarrow Mo(VI)$ in the binuclear species.

In the CV trace of the monomeric dioxidomolybdenum(VI) complex $[Mo^{VI}O_2L^5]$ (**5**), a single electron quasi-reversible response at $E_{1/2}$ value of −0.89 V and an irreversible reductive response at −1.69 V are observed (Figure 3b). The response at $E_{1/2} = -0.89$ V can be attributed to the $Mo(VI) \rightarrow Mo(V)$
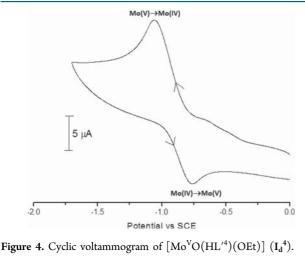
Figure 3. Cyclic voltammograms of (a) $[Mo_2^VO_2L'_2^4]$ (**4**) and (b) $[Mo^{VI}O_2L^5]$ (**5**).

reduction, while the peak at −1.69 V is due to the reduction of the salen type ligand.[53a]

The CV trace of I_d^4 (Figure 4) shows a single electron quasi-reversible reductive response at $E_{1/2}$ value of −0.91 V due to
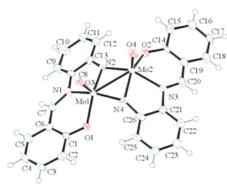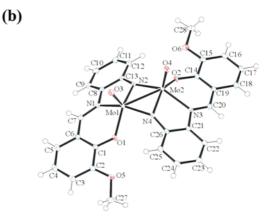

Figure 4. Cyclic voltammogram of $[Mo^VO(HL'^4)(OEt)]$ (I_d^4).

the reduction of Mo(V) → Mo(IV).[49f,53b,c] No metal centered oxidation peaks were observed during the anodic scans, indicating that I_d^4 is not electrochemically oxidizable to Mo(VI) species under these conditions.[49f,53b] An irreversible peak at 1.16 V is observed (Figure S8) which may be attributed to the oxidation of the ligand.[53d] Under identical experimental conditions, the single electron processes were verified by comparing its current height with that of the standard ferrocene−ferrocenium couple.

Description of X-ray Structure of Dinuclear Mo(V), $[Mo_2^VO_2L'_2^{1,2,4}]$ (1, 2, and 4), and Mononuclear Mo(VI), $[Mo^{VI}O_2L^5]$ (5), Complexes. The molecular structure of the dinuclear $[Mo_2^VO_2L'_2^{1,2,4}]$ (**1**, **2**, and **4**) and mononuclear $[Mo^{VI}O_2L^5]$ (**5**) complexes was determined by the single crystal X-ray diffraction technique, and ORTEP representations for the complexes are shown in Figure 5. The relevant bond distances and angles are collected in Tables 3 and 4.

The structures of **1**, **2**, and **4** contain dinuclear $[Mo_2^VO_2]^{6+}$ cores with Mo−Mo bonds. The rearranged ligands ($H_3L'^{1,2,4}$) coordinate each molybdenum atom through one phenoxido oxygen, one imino nitrogen, and one bridging imido nitrogen in a tridentate chelating manner (formation of $[Mo_2^VO_2L'_2^{1-4}]$

(**1−4**) is given in Scheme 2). Disregarding the metal−metal bond, each molybdenum atom exists in a distorted square-pyramidal geometry where the MoN_3O_2 coordination environment comprises two imido-bridged nitrogen atoms, one imino nitrogen atom, and one phenoxido oxygen atom describing the equatorial plane, and one oxido oxygen as an axial group. Distortion of the square plane is observed from the difference in the Mo−O(1)/O(2), Mo−N(1)/N(3), Mo−N(2), and Mo−N(4) bond lengths as well as the difference in the bond angles at the Mo atom [74.6(7) to 109.4(2)°]. The lengths of the Mo=O, Mo−O, $Mo-N_{imino}$, and $Mo-N_{imido}$ bonds are usual.[1,9e,49a−c,54] Both Mo acceptor centers are displaced from the average equatorial plane described by O(1)/O(2)−N(1)/N(3)−N(2)−N(4) toward the axial oxido oxygen atom O(3)/O(4) by about 0.63(1) Å, the distance of O(3)/O(4) from the same plane being about 2.3 Å. In the aldehyde oxidoreductase of *Desulfovibrio gigas*, similar displacement of the Mo atom from the equatorial plane toward the apical oxido oxygen atom is also found.[55] Due to this displacement, the Mo^V acceptor center becomes somewhat inaccessible to the donor approaching from the opposite direction. Therfore, it is evident that $[Mo_2^VO_2L'_2^{1-4}]$ (**1−4**) has a square-pyramidal structure with the sixth position, *trans* to the oxido oxygen atom O(3)/O(4), vacant. The shorter length of the $Mo-N_{imido}$ bond compared to the $Mo-N_{imine}$ bond indicates that the deprotonated bridging imido-N coordinates more strongly to the metal center than the imino group. The main reason for the structural distortion of complexes **1**, **2**, and **4** from the ideal geometry is their observed average bite angle of the tridentate ligands (79.15°), which are significantly deviated from 90°. The Mo(1)−Mo(2) bond distance in **1**, **2**, and **4** ranging between 2.64 and 2.66 Å indicates the formation of a localized metal−metal single bond.[1,3i,j,48b,c,56] Here, it is worth mentioning that this is the first structural evidence of metal−metal bonded oxidomolybdenum(V) complexes synthesized from salen type ligands containing an aromatic imine group. Earlier there have been reports on molybdenum complexes of similar ligands where molybdenum(VI) oxido[35a−c] or peroxido[35d] structures were proposed on the basis of assumptions from spectral data. However, the structures of **1**, **2**, and **4** clearly indicate that *in situ* hydrolysis and −C=N bond cleavage of one of the arms of the salophen ligands, containing an aromatic imine moiety, takes place in the presence of molybdenum acetylacetonate leading to the formation of dimeric oxidomolybdenum(V) complexes.
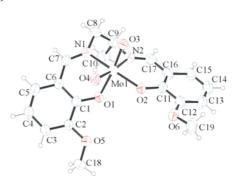
Figure 5. ORTEP representations of compounds (a) $[Mo_2^VO_2L'_2{}^1]$ (**1**), (b) $[Mo_2^VO_2L'_2{}^2]$ (**2**), (c) $[Mo_2^VO_2L'_2{}^4]$ (**4**), and (d) $[Mo^{VI}O_2L^5]$ (**5**) with displacement parameters of **1**, **2**, and **4** at 50% and **5** at 30% probability.

Table 3. Selected Bond Distances (Å) and Angles (deg) for Complexes 1, 2, and 4

	1	**2**	**4**
Bond Distances (Å)			
Mo1–O1	2.028(4)	2.016(2)	2.034(3)
Mo2–O2	2.020(5)	2.020(2)	2.035(5)
Mo1–O3	1.683(4)	1.693(2)	1.698(4)
Mo2–O4	1.687(5)	1.696(2)	1.703(4)
Mo1–N1	2.170(7)	2.167(2)	2.163(4)
Mo1–N2	1.947(5)	1.961(2)	1.974(4)
Mo2–N2	1.938(5)	1.962(2)	1.979(4)
Mo2–N3	2.175(5)	2.187(2)	2.153(4)
Mo1–N4	1.935(6)	1.948(2)	1.963(4)
Mo2–N4	1.955(5)	1.960(2)	1.966(4)
Mo1–Mo2	2.650(1)	2.656(3)	2.640(6)
Bond Angles (deg)			
O1–Mo1–N1	83.7(2)	82.7(7)	82.6(1)
O2–Mo2–N3	84.1(2)	82.9(6)	82.6(1)
O3–Mo1–O1	106.9(2)	108.5(7)	109.0(2)
O4–Mo2–O2	106.8(2)	109.2(7)	109.4(2)
N2–Mo1–N1	75.2(2)	75.7(7)	75.0(2)
N4–Mo2–N3	75.4(2)	74.6(7)	75.8(2)
Mo1–N2–Mo2	86.0(2)	85.2(7)	83.8(2)
Mo1–N4–Mo2	85.9(2)	85.6(7)	84.4(2)
N4–Mo1–O1	87.1(2)	85.7(7)	87.7(2)
N2–Mo2–O2	87.6(2)	86.8(7)	86.4(2)
O3–Mo1–Mo2	106.7 (2)	108.9(6)	105.4(1)
O4–Mo2–Mo1	105.6(2)	108.0(5)	105.4(1)

Table 4. Selected Bond Distances (Å) and Angles (deg) for Complex 5

bond distances (Å)		bond angles (deg)	
Mo1–O1	2.101(4)	O1–Mo1–N1	89.4(2)
Mo1–O2	1.918(4)	O2–Mo1–N2	167.0(2)
Mo1–O3	1.689(5)	O5–Mo1–N2	82.3(2)
Mo1–O4	1.701(5)	O4–Mo1–N2	167.0(2)
Mo1–N1	2.133(7)	N1–Mo1–N2	71.9(2)
Mo1–N2	2.279(8)	O1–Mo1–O2	102.9(2)

The mononuclear dioxidomolybdenum(VI) complex (**5**) shows a distorted octahedral geometry involving NO_3 donors as the basal plane occupied by one tertiary nitrogen N(1) and two phenolate oxygen atoms O(1) and O(2), all from the tetradentate ligand $(L^5)^{2-}$, together with a terminal oxido ligand O(3). Another terminal oxido oxygen atom O(4) and one tertiary nitrogen N(2), from the ligand, are attached to the metal atom to fill its two axial sites and form a *trans* O(4)–Mo–N(2) angle of 167.0(2)°. The Mo atom shifts 0.315(3) Å out of this mean meridional plane toward the O(4) atom. The rather long Mo–N distance 2.28(8) Å of the tertiary nitrogen N(2), from the ligand, to the sixth coordination position lying *trans* to the oxido-oxygen O(4) may be due to the displacement of the Mo atom from the equatorial mean plane toward O(4). The Mo–O(3) and Mo–O(4) bond distances of the $MoO_2{}^{2+}$ group are unexceptional.[38b,47e,57] All these structural features as well as bond length and angle values are in good accordance with similar *cis*-MoO_2L complexes of related N_2O_2 ligands reported earlier.[58a,b] The evaluation of structure of **5** involves application of SQUEEZE to remove the contribution of disordered solvent from the refinement, which was finished before the new SHELX version was available (see also the

related B-level CheckCIF alert). Also, recently a dioxidouranium(VI) complex with a similar tetradentate salen ligand as H_2L^5 has been reported in the literature where the metal is bound to the N_2O_2 donors in the same fashion.[58c]

DNA Binding Studies. In order to understand the binding of the molybdenum complexes **1**−**5** to CT-DNA, different spectroscopic techniques were used.

Absorption Spectroscopic Studies. The absorption bands of the complexes **1**−**5** originating in the regions 430−485 and 275−390 nm are attributed to L−Mo(dπ) LMCT and intraligand transitions, respectively.[49a] The equilibrium binding constant (K_b) of the complexes to CT-DNA was determined by UV−vis titration experiments (Table 5 and Figure 6). On

Table 5. DNA Binding Parameters for 1−5

complex	binding constant $(K_b)^a$ (M^{-1})	$\Delta T_m{}^b$ (°C)
1	2.50×10^4	+1.50
2	9.36×10^3	+1.00
3	8.44×10^3	+1.50
4	3.20×10^4	−2.00
5	9.90×10^4	+1.50

^{a}DNA binding constants were determined by the UV−vis spectral method. ^{b}Change in the melting temperature of CT-DNA.

addition of CT-DNA to the complex solution, the UV−vis absorption bands in the region 275−390 nm showed a hypochromic shift for **1**−**5** and an appreciable hyperchromic shift in the LMCT band for complex **5** (Figure 6). Both the hypochromism for **1**−**5** and hyperchromism for **5** indicate the interaction between the oxidomolybdenum complexes and CT-DNA. The hypochromic shift due to the intraligand transition for the complexes **1**−**5** was taken to calculate the binding affinity of the complexes with CT-DNA. The resulting hypochromicity of **1**−**5** in the intraligand transition band is possibly due to the interaction between the electronic states of the chromophores of the ligands and the DNA bases.[59−61a]

The binding affinity of the interaction between CT-DNA and each of the molybdenum complexes **1**−**5** is indicated by the binding constant, K_b, which was calculated using eq 1. The data reported in Table 5 reveal that the DNA binding strengths of the molybdenum complexes are in the order **5** > **4** > **1** > **2** > **3**, with the K_b values of **1**−**5** ranging from 9.90×10^4 to 8.44×10^3 M^{-1}. The binding affinity of the ligands to CT-DNA gave values lower than their corresponding molybdenum complexes (Figure S9 and Table S2). The order of the binding affinity can mainly be attributed to the small size of the complexes and incorporation of the electron donating groups attached to the aromatic rings in the ligands.[61b,c] Apart from this, both the phenyl and the naphthyl groups in these ligands may also play an important role in the interaction of the complexes with CT-DNA.[61d]

Thermal Denaturation Studies. In order to investigate the stability of the CT-DNA in the presence and absence of the molybdenum complexes **1**−**5**, DNA melting experiments were performed.[47a] The melting temperature (T_m) of CT-DNA in the absence of any complex was ∼66 °C, which is in accordance with our previous reports.[38c−g] Upon interaction with **1**−**3** and **5**, the T_m of CT-DNA increased very slightly (∼1.00−1.50 °C), whereas, upon interaction with **4**, the same was decreased slightly (∼2.0 °C) in Figure 7 and Table 5. The low ΔT_m values indicate that **1**−**3** and **5** may possibly bind to CT-DNA by groove binding mode rather than an intercalative mode, which

usually gives a large positive ΔT_m value.[62] Complex **4** showed a slightly negative ΔT_m value of −2.00 °C (Table 5 and Figure 7) possibly due to the destabilization of the DNA double helix.[63]

Circular Dichroism Studies. In order to study the conformational changes in CT-DNA upon the interaction with complexes, circular dichroism (CD) spectroscopy was used.[64] Two conservative CD bands in the UV region are observed for CT-DNA: a positive band at 275 nm due to base stacking interaction and a negative band at 245 nm due to right-handed helicity.[65a] Interaction of small molecules by groove binding mode shows less or no perturbation on the base stacking and helicity bands, whereas, during intercalation mode, intensity changes of both bands can be induced, therefore modulating the right-handed B-conformation of DNA.[64] The CD spectra of CT-DNA (100 μM) upon the interaction with **1**−**5** showed very minute changes, for the positive band at 275 nm as well as for the negative band at 245 nm (Figure S10), which suggests that the interaction of the oxidomolybdenum complexes **1**−**5** were groove binding (possibly minor groove binding mode) in nature. From the above DNA binding studies it may be depicted that the naphthyl group interacts with the DNA by groove binding mode, possibly by van der Waals forces of interaction, apart from this the naphthyl group can also interact with the DNA by hydrophobic interactions.[65b,c]

Competitive DNA Binding Studies. Competitive DNA binding studies by fluorescence measurements using DAPI could not be performed as the complexes **1**−**4** as well as the ligands H_2L^{1-4} exhibited an intense fluorescence in the same region. In order to assess the major groove and intercalative binding mode, competitive binding experiments were carried out with methyl green (MG) and ethidium bromide (EB), respectively.[38e] But, we did not observe any quenching in the fluorescence of MG and EB bound to CT-DNA (672 and 597 nm, respectively) upon the successive addition of the complexes **1**−**5**.[38e] Hence, the complexes do not interact with CT-DNA either by major groove or intercalative mode of binding. In another way, these two competitive binding results hinted toward the possibility of interaction of these complexes with the CT-DNA via minor groove binding mode. In fact, thermal denaturation and circular dichroism findings also indicated a similar possibility, i.e., the complexes **1**−**5** possibly interact with the CT-DNA by minor groove binding mode.

DNA Cleavage Studies. *Chemically Induced DNA Cleavage.* The chemically induced DNA cleavage activity of **1**−**5** (1−100 μM) was performed in the dark, using supercoiled pUC19 DNA (300 ng) in 50 mM Tris−HCl buffer (pH 8.0) in 1% DMF, in the presence of hydrogen peroxide (500 μM) as the oxidizing agent. The molybdenum complexes do not exhibit any chemically induced DNA cleavage activity.

Photoinduced DNA Cleavage. To evaluate whether **1**−**5** possess photonuclease activity, a photoinduced DNA cleavage activity assay was carried out. The photoinduced DNA nuclease activity of **1**−**5** on irradiation of UVA light of 350 nm for 3 h in the absence and presence of the complexes was studied using supercoiled (SC) pUC19 DNA (300 ng) in 50 mM Tris−HCl buffer (pH 8.0) containing 1% DMF (Figure S11). The extent of the DNA cleavage was confirmed by the decrease in the supercoiled pUC19 DNA (form I) and subsequent formation of nicked circular DNA (form II) and linear DNA (form III). The percentage of net DNA cleavage by the complexes was estimated using the following equation:
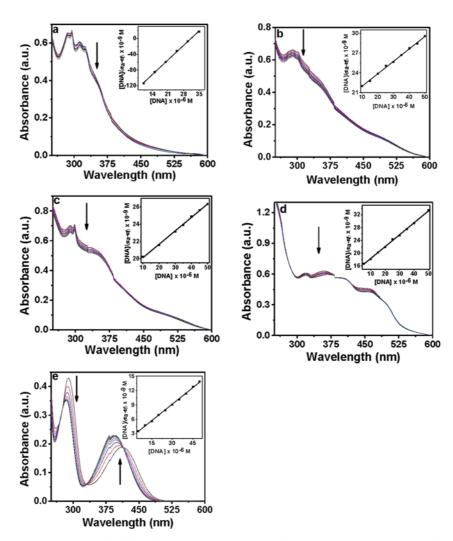
Figure 6. Electronic absorption spectra of **1** (a), **2** (b), **3** (c), **4** (d), and **5** (e) (25 μM) upon the titration of CT-DNA (0−50 μM). The experiments were performed in 10 mM Tris−HCl buffer (pH 8.0) containing 1% DMF. Arrow indicates the changes in absorbance with respect to an increase in the CT-DNA concentration. The linear fit of $[DNA]/(\varepsilon_a - \varepsilon_f)$ vs $[DNA]$ is given in the inset. The binding constant (K_b) was calculated using eq 1.
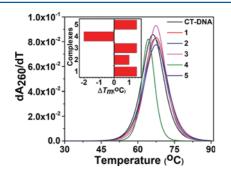

Figure 7. Derivative plot of thermal denaturation of CT-DNA (100 μM) in the absence and presence of **1−5** (25 μM) in 10 mM Tris−HCl buffer (pH 8.0) containing 1% DMF. The ΔT_m (°C) of the complexes as compared to CT-DNA is shown in the inset.

Net DNA cleavage %

$$= \frac{\text{form II}_s + 2 \times \text{form III}_s}{\text{form I}_s + \text{form II}_s + 2 \times \text{form III}_s}$$
$$- \frac{\text{form II}_c + 2 \times \text{form III}_c}{\text{form I}_c + \text{form II}_c + 2 \times \text{form III}_c} \quad (2)$$

The subscripts s and c refer to the sample and control, respectively.[65] Since we did not observe a DNA band corresponding to form III in our photonuclease studies, the concentration of form III is put as zero for both "control" and "sample". The DNA cleavage activity of the molybdenum complexes **1−5** was carried out in a concentration dependent manner from 1 to 100 μM. The net DNA cleavage percent by **1−5** was plotted with increasing concentration of the molybdenum complexes (Figure 8). Approximately 1−5% DNA cleavage was observed in the presence of 1 μM of **1−3** and **5** whereas at the same concentration **4** showed a DNA cleavage of ~37% (Figure 8). The DNA cleavage activity for each of the complexes was saturated at a concentration of 50 μM. At this concentration, the photonuclease activity of **1**, **2**, **3**, **4**, and **5** was approximately, 17, 26, 36, 93, and 4%, respectively. This indicated that **4** has the most promising photonuclease activity among the complex series. Cleavage activity of **1−5** varies due to the different functional groups present in the ligand moieties.[38c−g] Complex **4** exhibits the highest photonuclease activity, which may be due to the presence of extended aromatic ring on the naphthyl group[61d] present in the ligand moiety. Apart from this, the presence of the phenyl group and the electron donating groups on the aromatic rings might also influence the DNA cleavage activity of the complexes.[61c] From
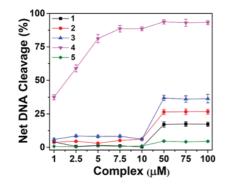
12

Figure 8. Concentration dependent DNA cleavage of **1−5**; 300 ng of SC pUC19 DNA at different concentration of the complexes [1−100 μM in 50 mM Tris−HCl buffer (pH 8.0) containing 1% DMF] was photoirradiated with UVA at 350 nm for 3 h. The net DNA cleavage percent was determined using eq 2. Each of the data points measured is mean ± standard deviation from triplicate experiments.

the control experiments it could be concluded that neither DMF (1%) nor the ligand molecules $H_2L^{1−3}$ and H_2L^5, at a concentration of 50 μM, showed any photoinduced DNA cleavage activity, implying that DMF and the ligands $H_2L^{1−3}$ and H_2L^5 are cleavage inactive under similar experimental conditions (Figure S12). However, the ligand molecule H_2L^4, at a concentration of 50 μM, showed a DNA cleavage activity of ∼20% (Figure S12), which increased significantly upon complexation (∼93% at a 50 μM complex concentration) to molybdenum (Figure 8). This indicated that the better activity of complex **4** was due to the presence of naphthyl moiety in the ligand H_2L^4.[66a]

The photoinduced DNA cleavage activity of **1−5** was examined in the presence of various additives, to discern the mechanistic pathways of the photocleavage reactions. There can be two possible mechanistic pathways by which the DNA cleavage reaction proceeds, which involve molecular oxygen: (i) a type II process where a singlet oxygen species ($^1O_2$) is involved or (ii) a photoredox process where reactive hydroxyl radicals ($^•OH$) are involved.[66b] When NaN_3 (a singlet oxygen quencher) was added, the DNA cleavage activity of **4** was inhibited by ∼24%, while in the presence of KI (a hydroxyl radical quencher), it was inhibited by ∼54% (Figure S13 and Figure S14). Further, in the presence of L-histidine (singlet oxygen quencher) and D-mannitol (hydroxyl radical quencher), the DNA cleavage activity of **4** was restrained by ∼14 and ∼19%, respectively (Figure S13 and Figure S14). However, no inhibition of DNA cleavage was observed for **1−3** and **5** in the presence of the additives (Figure S13). Therefore, it can be concluded that **4** exhibits photoinduced DNA cleavage activity probably via both singlet oxygen and hydroxyl radical pathways. However, the mechanistic pathways associated with the photoinduced DNA cleavage by **1−3** and **5** cannot be distinctly ascertained.

The above results of the DNA interaction studies of the synthesized molybdenum complexes **1−5** are in accordance with previous reports of DNA binding/cleavage studies of related oxidomolybdenum(VI)[67a−d] and those of other transition metal[67e−h] salen complexes. However, the DNA cleavage activity of complex **4** (∼93% at a 50 μM complex concentration) is exceptionally better than in the previous reports.

Cytotoxicity Studies. *MTT Assay.* The antiproliferative efficacy of **1−5** was assayed by determining the viability of

MCF-7 (human breast adenocarcinoma) and HCT-15 (colon cancer) cells using the MTT assay as per our previous protocol.[67i,j] The ligands $H_2L^{1−5}$ and $MoO_2(acac)_2$ gave high IC_{50} values (>200 μM), whereas **1−5** gave values in the range 28.52−11.13 μM in MCF-7 cells and between 76.30 and 32.20 μM in HCT-15 cells (Table 6). In contrast, cisplatin, a widely

Table 6. Cytotoxicity of 1−5 as Measured by MTT Assay in MCF-7, HCT-15, and HaCaT Cells

complex	IC_{50}[a] (μM)		
	MCF-7	HCT-15	HaCaT
1	11.13 ± 0.65	32.20 ± 0.92	200.74 ± 0.12
2	13.25 ± 1.32	52.54 ± 2.68	179.47 ± 1.02
3	28.52 ± 2.65	76.30 ± 1.84	477.26 ± 2.36
4	12.43 ± 0.94	54.92 ± 1.06	370.13 ± 0.51
5	27.31 ± 1.83	55.61 ± 0.65	96.00 ± 0.09

[a]Values are mean ± SD, n = 3.

used chemotherapeutic drug, is comparatively effective in MCF-7[68a] and HCT-15[68b] cells with an IC_{50} value of 7.8 and 12.20 μM respectively. The marked decrease in the inhibitory ability of $H_2L^{1−4}$ as well as their lower binding propensity to CT-DNA compared to **1−5** indicates that incorporation of molybdenum has a significant effect on cytotoxicity. This is possibly because the polarity of the ligand and the central metal ion is reduced by coordination through the charge equilibration. This favors the permeation of the complexes through the lipid layer of the cell membrane.[68c,69] The results of DNA binding/cleavage ability for the ligands as well as the complexes also indicate that the metal complexes exhibit greater biological activities than the free ligands.[70]

The cytotoxic activities of the complex series **1−5** can be judged from their IC_{50} values (Table 6), with their dose dependency illustrated in Figures 9 and 10.
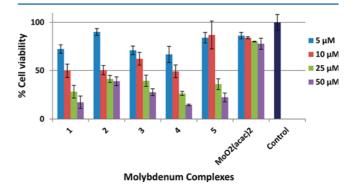

Figure 9. Effect of the complexes (**1−5**) on cell viability and growth of MCF-7 cells. The cells were treated with different concentrations of the test compounds for 48 h, and then cell viability was calculated by MTT assay. Data reported as the mean ± SD for n = 3.

IC_{50} values of the complexes **1**, **4**, and **2** ranges between 11.13 and 13.25 μM in the case of MCF-7, and in the case of HCT-15 it ranges between 32.20 and 54.92 μM, while **3** and **5** have IC_{50} values in the range 27.31−28.52 μM in the case of MCF-7 and between 55.61 and 76.30 in HCT-15 cells. Since the variation in the IC_{50} values obtained for complexes **1**, **4**, and **2** is somewhat different from that of **3** and **5**, these complexes can be combined into two groups, i.e., "group 1" corresponding to the complexes with higher cytotoxicity (**1**, **4**, and **2**) and
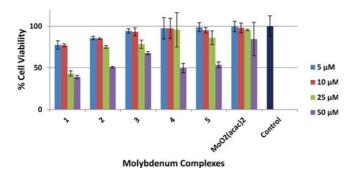
13

Figure 10. Effect of the complexes (1−5) on cell viability and growth of HCT-15 cells. The cells were treated with different concentrations of the test compounds for 48 h and then cell viability was calculated by MTT assay. Data reported as the mean ± SD for $n = 3$.

"group 2" corresponding to the complexes with lower cytotoxicity (3 and 5). The cytotoxicity order of the complexes matches completely neither with the DNA binding order nor with the photonuclease activity order. However, group 1 complexes, with higher cytotoxicity, do exhibit comparatively higher photonuclease activity than group 2 complexes, which have lower cytotoxicity. The variation in results of cytotoxicity of the complexes may be affected by the various functional groups in the salen ligands. The presence of the electron withdrawing Br group in complex 3 leads to an increase in the IC$_{50}$ (less cytotoxicity),[18] while complex 1, which has no substituents on the ligand fragment, and complex 2, which contains an electron releasing −OMe group, exhibit lower IC$_{50}$ (higher cytotoxicity).[18] The considerable efficacy of 4 in MCF-7 cells, as also inferenced from DNA binding/cleavage studies, may be due to the presence of the naphthyl group in the ligand

moiety.[66a] Also, the introduction of aromatic diimine bridges in the salen complexes (1, 2, and 4) increases their cytotoxicity, as evident from the higher IC$_{50}$ value of complex 5 (less cytotoxicity), which contains an aliphatic diimine bridge.[22c]

The MTT assay for determining the cytotoxicity of metal complexes on the HaCaT (immortalized human keratinocytes) cell line was also performed. The very high IC$_{50}$ values of 1−5 (96.00−477.26 μM, Table 6) and their dose dependency (Figure S15) in HaCaT cells indicated that the compounds exhibited no substantial cytotoxicity to normal keratinocytes.

In the recent past, some oxidomolybdenum(VI) complexes have been reported to have significant cytotoxic activities against various human cancer cell lines including HL-60 and K562 (leukemia), A-549 (lung cancer), HeLa (cervical carcinoma), and MCF-7 (breast carcinoma).[24,34,67b,71] Salen complexes of some transition metals have also been reported to show appreciable cytotoxic activities against human cancer cell lines.[22a,c,72] In few cases the results of the above studies are in accordance with the synthesized molybdenum complexes 1−5, while in some cases they exhibit better cytotoxicity than 1−5 in terms of IC$_{50}$ values.

Nuclear Morphological Studies. Investigation of apoptotic potential of compounds is usually performed by DAPI staining experiments.[38c−g] However, it was found that the synthesized molybdenum complexes 1−4 themselves exhibited fluorescence emission at the same wavelengths as DAPI (blue region). Hence, the use of DAPI as staining agent was inappropriate in the present situation, and therefore it was replaced by propidium iodide, which exhibited red fluorescence, to examine the effect of the test complexes on nuclear morphology of MCF-7 and HCT-15 cells. To check the live cells in different treatment groups, the density of the PI stained nuclei was used. Figure 11 and Figure 12 show images taken after PI staining in
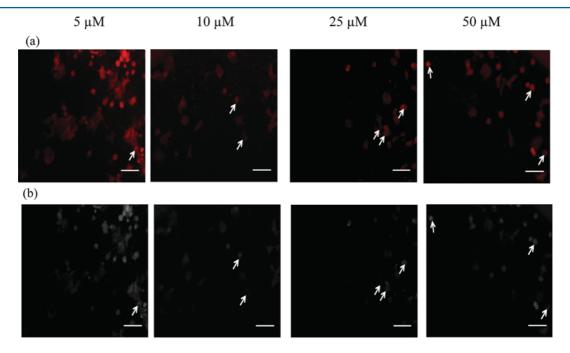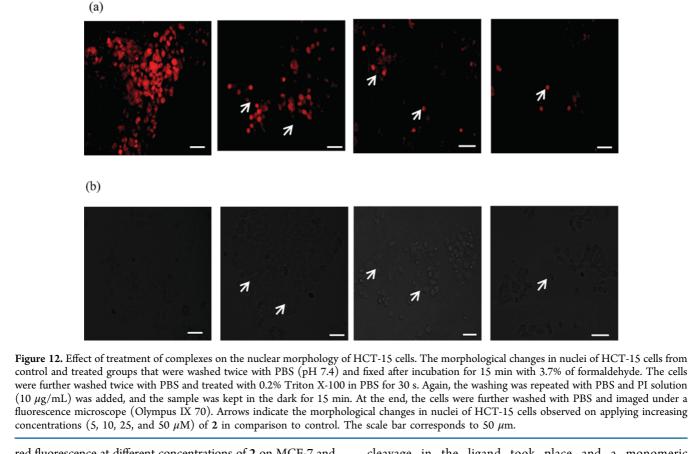

Figure 11. Effect of treatment of complexes on the nuclear morphology of MCF-7 cells. The morphological changes in nuclei of MCF-7 cells from control and treated groups that were washed twice with PBS (pH 7.4) and fixed after incubation for 15 min with 3.7% of formaldehyde. The cells were further washed twice with PBS and treated with 0.2% Triton X-100 in PBS for 30 s. Again, the washing was repeated with PBS and PI solution (10 μg/mL) was added, and the sample was kept in the dark for 15 min. At the end, the cells were further washed with PBS and imaged under a fluorescence microscope (FLoid, Life Technologies). Arrows indicate the morphological changes in nuclei of MCF-7 cells observed on applying increasing concentrations (5, 10, 25, and 50 μM) of 2 in comparison to control. The scale bar corresponds to 100 μm.

Figure 12. Effect of treatment of complexes on the nuclear morphology of HCT-15 cells. The morphological changes in nuclei of HCT-15 cells from control and treated groups that were washed twice with PBS (pH 7.4) and fixed after incubation for 15 min with 3.7% of formaldehyde. The cells were further washed twice with PBS and treated with 0.2% Triton X-100 in PBS for 30 s. Again, the washing was repeated with PBS and PI solution (10 μg/mL) was added, and the sample was kept in the dark for 15 min. At the end, the cells were further washed with PBS and imaged under a fluorescence microscope (Olympus IX 70). Arrows indicate the morphological changes in nuclei of HCT-15 cells observed on applying increasing concentrations (5, 10, 25, and 50 μM) of **2** in comparison to control. The scale bar corresponds to 50 μm.

red fluorescence at different concentrations of **2** on MCF-7 and HCT-15 cells, respectively. Figures S16 and S17 show images taken after PI staining of **1** and **3−5** on MCF-7 and HCT-15 cells, respectively. It is observed from the figures that the number of PI stained nuclei was reduced in treated wells with increasing concentrations of **1−5**, indicating dose dependent cell death.[73,74] The gray scale images at 48 h after the treatment with increasing concentrations of **1−5** are shown in Figure 11b and Figure 12b for MCF-7 and HCT-15 cells, respectively. The distinct nuclear condensation and fragmentation (indicated by arrows) were seen in treated cells (Figures 11 and 12) compared to control cells (Figures S16A and S17A).

■ CONCLUSIONS

Five salen type ligands from an aromatic diamine, *o*-phenylenediamine (H$_2$L$^{1−4}$), and an aliphatic diamine, 1,2-diaminopropane (H$_2$L^5), were synthesized. H$_2$L$^{1−4}$ furnished dimeric bis-μ-imido bridged oxidomolybdenum(V) complexes [Mo$_2^V$O$_2$L$'_2^{1−4}$] (**1−4**), where L$'^{1−4}$ indicates the rearranged form of the ligands H$_2$L$^{1−4}$, via an interesting mechanistic pathway which involves the formation of rare monomeric molybdenum(V) intermediate [Mo^{V}O(HL$'^{1−4}$)(OEt)] (**I$_d^{1−4}$**) by the molybdenum assisted hydrolysis of the imine bond and subsequent −C≡N bond cleavage of the salophens. The deprotonation and dimerization of Mo(V) intermediates finally resulted in the formation of two imido bridges between the Mo(V) centers containing a metal−metal bond. One of the molybdenum(V) intermediates, [Mo^{V}O(HL$'^4$)(OEt)] (**I$_d^4$**), was isolated in the solid state and characterized by spectral (IR, UV−vis, EPR), ESI-MS, and cyclic voltammetry studies. In the case of H$_2$L^5, no such imine hydrolysis or −C≡N bond

cleavage in the ligand took place and a monomeric dioxidomolybdenum(VI) complex [Mo^{VI}O$_2$L^5] (**5**) was furnished. The structures of dimeric metal−metal bonded oxidomolybdenum(V) complexes synthesized from salen type ligands containing aromatic imines were established for the first time through X-ray crystallography, and the mechanistic pathway of their formation was also explained. The disappearance of EPR signals in the Mo(V) intermediate **I$_d^4$** after 30 min also proved the formation of corresponding diamagnetic dimeric bis-μ-imido bridged oxidomolybdenum(V) complexes, where antiferromagnetic coupling[48a] occurs between the two Mo(V) centers. Comparison with several other transition metal complexes of similar ligand systems,[41] where no such ligand transformation takes place, proved that the hydrolysis and −C≡N bond cleavage of salophen ligands was Mo assisted.

In vitro biological studies reveal that **1−5** show appreciable DNA binding propensity. The CD and thermal melting studies revealed that the complexes possibly interact with CT-DNA in a manner consistent with groove binding mode, with binding constants ranging from 10^3 to 10^4 M$^{−1}$. **1−5** exhibited good photoinduced cleavage of pUC19 supercoiled plasmid DNA, with **4** giving the maximum photoinduced DNA cleavage activity of ~93%. It is concluded from the mechanistic study that the photolytic DNA cleavage of **4** proceeded via both singlet oxygen and hydroxyl radical pathways, whereas the mechanistic pathways associated with **1−3** and **5** could not be distinctly ascertained. Also, results of antiproliferative activities of the synthesized complexes suggested that they are significantly cytotoxic toward MCF-7 and HCT-15 cell lines. The complexes containing the aromatic diimine moiety (**1**, **2**,

and **4**) were found to be more cytotoxic than the complex containing the aliphatic diimine (**5**). The presence of the electron withdrawing Br group in **3** lowered its cytotoxicity. The better activity of **4** may be attributed to the presence of the naphthyl moiety in the ligand system. Also, **1−5** did not exhibit significant cytotoxicity to HaCaT cells (immortalized human keratinocytes). The present results will encourage further work on oxidomolybdenum complexes for the development of metal-based agents for anticancer studies.

■ ASSOCIATED CONTENT

Ⓢ Supporting Information

The Supporting Information is available free of charge on the ACS Publications website at DOI: 10.1021/acs.inorg-chem.7b01578.

> ^{1}H NMR, UV−vis, FTIR, ESI-MS, absorbance, and CD spectra, binding constant values, absorption spectral traces, cyclic voltammogram, electronic absorption spectra, and gel diagrams (PDF)

Accession Codes

CCDC 1491689−1491692 contain the supplementary crystallographic data for this paper. These data can be obtained free of charge via www.ccdc.cam.ac.uk/data_request/cif, or by emailing data_request@ccdc.cam.ac.uk, or by contacting The Cambridge Crystallographic Data Centre, 12 Union Road, Cambridge CB2 1EZ, UK; fax: +44 1223 336033.

■ AUTHOR INFORMATION

Corresponding Author

*E-mail: rupamdinda@nitrkl.ac.in.

ORCID Ⓞ

Alok K. Panda: 0000-0002-4452-993X
Eugenio Garribba: 0000-0002-7229-5966
Rupam Dinda: 0000-0001-9452-7791

Notes

The authors declare no competing financial interest.

■ REFERENCES

(1) Modec, B.; Brenčič, J. V.; Koller, J. A Series of Molybdenum(V) Complexes with the Oxalato Ligand Engaged in Different Binding Roles − An Unusual Staggered Conformation of the μ_4-Oxalate in [{Mo$_2$O^4(η^2-C$_2$O$_4$)$_2$}2(μ_4-C$_2$O$_4$)]$^{6-}$. *Eur. J. Inorg. Chem.* **2004**, *2004*, 1611−1620.

(2) Modec, B.; Brenčič, J. V. From Small {Mo$_2$O$_4$}$^{2+}$ Aggregates to Infinite Solids. *J. Cluster Sci.* **2002**, *13*, 279−302.

(3) (a) Delbaere, L. T. J.; Prout, C. K. The X-ray Crystal and Molecular Structure of a Molybdenum(V)-L-Histidine Complex Mo$_2$O$_4$(L-histidine)$_2$,3H$_2$O. *J. Chem. Soc. D* **1971**, *0*, 162−162. (b) Beaver, J. A.; Drew, M. G. B. Crystal and Molecular Structure of Tetrachloro-di-μ_3-oxo-tetra-μ-prop-oxo-tetraoxodipropoxotetramolybdenum(2MO−MO). *J. Chem. Soc., Dalton Trans.* **1973**, 1376−1380. (c) Modec, B.; Brenčič, J. V.; Golič, L.; Giester, G. Oxomolybdenum Coordination Compounds with Pyridine. Syntheses and Structures of [Mo$_4$O$_8$(OCH$_3$)2Cl$_2$L$_4$]·2L (L = Py, 4-MePy), [Mo$_4$O$_8$(OCH$_3$)$_4$(4-MePy)$_4$], [Mo$_6$O$_{12}$(OCH$_3$)6Py$_4$] and [Mo$_{10}$O$_2$6Py$_8$]·7Py. *Inorg. Chim. Acta* **2000**, *307*, 33−41. (d) Zhou, Z.; Xu, Q.; Lin, J.; Ng, S.-W. pH Dependent Formations of Dinuclear Molybdenum(V) and Incomplete Cubane Molybdenum(IV) Complexes with Nitrilotriacetate. *Inorg. Chem. Commun.* **2007**, *10*, 1461−1464. (e) Modec, B.; Brenčič, J. V. Novel Hydrogenmaleato Molybdenum(V) Complexes Based on a Dinuclear Metal−Metal Bonded Unit: Syntheses and Structural Characterization of (PyH)$_3$[Mo$_2$O$_4$Cl$_4$(OOCCH = CHCOOH)] and (PyH)$_3$[Mo$_2$O$_4$Br$_4$(OOCCH═CHCOOH)] CH$_3$CN. *Inorg. Chem. Commun.* **2004**, *7*, 516−520. (f) Zhou, Z.-H.; Deng, Y.-F.; Cao, Z.-X.; Zhang, R.-H.; Chow, Y. L. Dimeric Dioxomolybdenum(VI) and Oxomolybdenum(V) Complexes with Citrate at Very Low pH and Neutral Conditions. *Inorg. Chem.* **2005**, *44*, 6912−6914. (g) Modec, B.; Dolenc, D. Molybdenum(V) Complexes with Formate: Geometric Isomerism of the [Mo$_2$O$_4$Cl$_2$(Py)$_2$(HCOO)]$^-$ Ion. *J. Mol. Struct.* **2013**, *1051*, 354−360. (h) Shibahara, T.; Ogasahara, S.; Sakane, G. catena-Poly[[diaquazinc(II)]-μ-L-cysteinato(2−)-κ^4S:S,N,O-[di-μ-sulfido-bis[oxidomolybdate(V)](Mo−Mo)]-μ-L-cysteinato(2−)-κ^4S,N,O:S]. *Acta Crystallogr., Sect. E: Struct. Rep. Online* **2008**, *64*, m605−m606. (i) Wu, P.-F.; Li, D.-S.; Meng, X.-G.; Zhong, X.-L.; Jiang, C.; Zhu, Y.-L.; Wei, Y.-G. Di-μ-oxo-bis[(histidinato-κ^3N,N,O)-oxomolybdenum(V)] Trihydrate. *Acta Crystallogr., Sect. E: Struct. Rep. Online* **2005**, *61*, m1553−m1555. (j) Tašner, M.; Prugovečki, B.; Soldin, Z.; Prugovečki, S.; Rukavina, L.; Matković-Čalogović, D. Synthesis and Characterization of Oxomolybdenum(V) Dinuclear Complexes with β-Alanine, $_L$-Serine and $_{DL}$-Isoleucine. *Polyhedron* **2013**, *52*, 268−275. (k) Meienberger, M. D.; Morgenstern, B.; Stucky, S.; Hegetschweiler, K. Polymerization of Mo^V: Synthesis and Characterization of a Dinuclear Mo^V and a Hexanuclear Mixed-Valence Mo^V/Mo^{VI} Complex. *Eur. J. Inorg. Chem.* **2008**, *2008*, 129−137. (l) Cindrić, M.; Pavlović, G.; Vrdoljak, V.; Kamenar, B. Hexanuclear Complexes of Molybdenum(V) Containing [Mo$_6$O$_{12}$(OCH$_3$)$_4$(acac)$_3$]$^-$ Anion. *Polyhedron* **2000**, *19*, 1471−1478. (m) Majumdar, M.; Patra, S. K.; Bera, J. K. Oxidative Route to Polyoxomolybdates from Quadruply Bonded [Mo^{II}≡Mo^{II}] Precursor: Structural Characterization of a Tetranuclear Cluster [Mo$_4$Cl$_5$O$_8$(pyNP)$_2$] (pyNP = (2-(2-pyridyl)1,8-naphthyridine)). *Polyhedron* **2007**, *26*, 1597−1602. (n) Sreehari, S.; Luck, R. L. *J. Cluster Sci.* **2010**, *21*, 525−541.

(4) (a) Hsieh, T.-C.; Gebreyes, K.; Zubieta, J. Studies of Molybdenum Thiolato-Complexes. The Chemical Characterization and the Crystal and Molecular Structures of Two Sulphido-Bridged Mo^V Dimers, [PhCH$_2$PPh$_3$]$_2$[Mo$_2$O$_2$S$_2$(SC$_2$H$_4$S)$_2$] and [HNEt$_3$]$_2$[Mo$_2$S$_4$(SC$_2$H$_4$S)$_2$]. *Transition Met. Chem.* **1985**, *10*, 81−84. (b) Martinez, M.; Ooi, B.-L.; Sykes, A. G. Reaction Paths in the Formation of Triangular and Cuboidal Molybdenum/Sulfur Cluster Complexes as Aqua Ions by Reduction of Molybdenum(V) Dimers. *J. Am. Chem. Soc.* **1987**, *109*, 4615−4619. (c) Koffi-Sokpa, E. I.; Calfee, D. T.; Allred, B. R. T.; Davis, J. L.; Haub, E. K.; Rich, A. K.; Porter, R. A.; Mashuta, M. S.; Richardson, J. F.; Noble, M. E. Activation of Ligand Reactivity: Thiolate C−S and Dithiophosphate Ester C−O Heterolyses within a Dimolybdenum(V) System. *Inorg. Chem.* **1999**, *38*, 802−813. (d) Cindrić, M.; Matković-Čalogović, D.; Vrdoljak, V.; Kamenar, B. Synthesis and Characterization of a Series of New Thiocarboxylate Complexes of Molybdenum(V). *Inorg. Chim. Acta* **1999**, *284*, 223−228. (e) Yoshida, R.; Ogasahara, S.; Akashi, H.; Shibahara, T. Crystal Structural Diversity of Sulfur-Bridged Cysteinato Dimolybdenum(V) Complexes: The Influence of Counter Metal Cations. *Inorg. Chim. Acta* **2012**, *383*, 157−163. (f) Xu, J.-Q.; Zhou, X.-H.; Zhou, L.-M.; Wang, T.-G.; Huang, X.-Y.; Averill, B. A. The First Binuclear Mo−S Cluster Compound Containing Citrate Ligands, K$_5$(NH$_4$)[Mo$_2$O$_2$(μ-S)$_2$(C$_6$H$_4$O$_7$)$_2$]·CH$_3$OH·5H$_2$O, Characterized by X-ray Single Crystal Structure Determination. *Inorg. Chim. Acta* **1999**, *285*, 152−154.

(5) (a) Chakrahari, K. K. V.; Dhayal, R. S.; Ghosh, S. Synthesis and characterization of binuclear μ-oxo and μ-telluro molybdenum(V)

complexes, $[Cp*Mo(O)(\mu\text{-Te})]_2$. *Polyhedron* **2011**, *30*, 1048−1054. (b) Sattler, A.; Parkin, G. Trinuclear, Tetranuclear and Octanuclear Chalcogenido Clusters of Molybdenum and Tungsten Supported by Trimethylphosphine Ligands. *Polyhedron* **2014**, *84*, 74−86.

(6) Bortoluzzi, M.; Hayatifar, M.; Marchetti, F.; Pampaloni, G.; Zacchini, S. Synthesis of Di- and Tetranuclear Oxido-Molybdenum(V) Complexes Containing p-Toluenesulfonates as Ligands: a Joint Spectroscopic, Crystallographic and Computational Study. *Dalton Trans.* **2014**, *43*, 10157−10163.

(7) Bazhenova, T. A.; Lyssenko, K. A.; Kuznetsov, D. A.; Kovaleva, N. V.; Manakin, Y. V.; Savinykh, T. A.; Shestakov, A. F. Methanolysis of $MoCl_5$ in the Presence of Different Alkaline Agents; Molecular Structures of the Polynuclear Molybdenum(V) Methoxides and Electron Charge Density Distribution From X-ray Diffraction Study of the New K−Mo Cluster. *Polyhedron* **2014**, *76*, 108−116.

(8) (a) Spivack, B.; Dori, Z. Structural Aspects of Molybdenum(IV), Molybdenum(V) and Molybdenum(VI) Complexes. *Coord. Chem. Rev.* **1975**, *17*, 99−136. (b) Chae, H. K.; Klemperer, W. G.; Paez-Loyo, D. E.; Day, V. W.; Eberspacher, T. A. Synthesis and Structure of a High Nuclearity Oxomolybdenum(V) Complex, $[(C_5Me_5Rh^{III})8\text{-}(Mo^V_{12}O_{36})(Mo^{VI}O_4)]^{2+}$. *Inorg. Chem.* **1992**, *31*, 3187−3189. (c) Chae, H. K.; Klemperer, W. G.; Marquart, T. A. High-nuclearity oxomolybdenum(V) complexes. *Coord. Chem. Rev.* **1993**, *128*, 209−224.

(9) (a) Amor, F.; Gómez-Sal, P.; de Jesús, E.; Martín, A.; Pérez, A. I.; Royo, P.; Vázquez de Miguel, A. Dimetallic Imido Complexes of Molybdenum and Tungsten with Bridged Bis(η5-cyclopentadienyl) Ligands. Molecular Structure of $[(MoO)_2(\mu\text{-N}^t\text{Bu})_2\{\mu\text{-}(\eta^5\text{-}C_5H_4)_2SiMe_2\}]$. *Organometallics* **1996**, *15*, 2103−2107. (b) Mathur, P.; Ghose, S.; Hossain, M. M.; Vahrenkamp, H. Synthesis and Structural Characterization of a New μ_2-Te Bridged Complex of Molybdenum with Oxo and Imido Ligands. *J. Organomet. Chem.* **1997**, *538*, 185−188. (c) Edelblut, A. W.; Wentworth, R. A. D. Formation of $Mo_2O_3(NH)(S_2P(OEt)_2)_2$, A Complex with a Bridging Imido Ligand, and its Reactions with Acids. *Inorg. Chem.* **1980**, *19*, 2006−2010. (d) Fletcher, J.; Hogarth, G.; Tocher, D. A. Dimolybdenum Oxo-Imido Complexes: Reactivity of $[(MeC_5H_4)_2Mo_2O_2(\mu\text{-O})(\mu\text{-NPh})]$ and Crystal Structure of $[(MeC_5H_4)_2Mo_2O(S)(\mu\text{-O})(\mu\text{-NPh})]$. *J. Organomet. Chem.* **1991**, *405*, 207−215. (e) Margulieux, G. W.; Turner, Z. R.; Chirik, P. J. Synthesis and Ligand Modification Chemistry of a Molybdenum Dinitrogen Complex: Redox and Chemical Activity of a Bis-(imino)pyridine Ligand. *Angew. Chem., Int. Ed.* **2014**, *53*, 14211−14215.

(10) (a) Murdzek, J. S.; Schrock, R. R. Well-Characterized Olefin Metathesis Catalysts that Contain Molybdenum. *Organometallics* **1987**, *6*, 1373−1374. (b) Nugent, W. A. Synthesis of some d⁰ Organoimido Complexes of the Early Transition Metals. *Inorg. Chem.* **1983**, *22*, 965−969. (c) Ma, Y.; Demou, P.; Faller, J. W. A Tungsten-183 NMR study of Mononuclear tungsten(VI) Methyl Complexes Containing Terminal oxo, sulfido, and imido ligands. *Inorg. Chem.* **1991**, *30*, 62−64. (d) Dahl, L. F.; Frisch, P. D.; Gust, G. R. Synthesis, Structure, and Bonding of a Sulfur-Bridged Alkyl Imido Dimeric Complex of Molybdenum(V). *J. Less-Common Met.* **1974**, *36*, 255−264. (e) Hansen, N. A. K.; Herrmann, W. A. Controlled Thermolysis of Nitrido- and Imidomolybdenum Complexes: A New Route to Phase-Pure Molybdenum Nitrides. *Chem. Mater.* **1998**, *10*, 1677−1679. (f) Coffey, T. A.; Forster, G. D.; Hogarth, G. Synthesis and Molecular Structure of the Molybdate-Bridged Cyclic Imido Complex $[Mo(S_2CNEt_2)_2(NR)(\mu\text{-MoO}_4)]_2$ (R = 2, 6-^{i}Pr$_2$C$_6$H$_3$). *Inorg. Chim. Acta* **1998**, *274*, 243−246. (g) Topaloglu-Sozuer, I.; Dulger Irdem, S.; Jeffery, J. J.; Hamidov, H. Synthesis, Spectroscopic Characterization and X-ray Crystal structures of Oxo-Bridged Oxo(haloaryl) Imido Hydrotris(3, 5-dimethylpyrazolyl) borate Molybdenum(V) Complexes. *J. Coord. Chem.* **2005**, *58*, 175−187. (h) Arae, S.; Nakajima, K.; Takahashi, T.; Ogasawara, M. Enantioselective Desymmetrization of 1,2,3-Trisubstituted Metallocenes by Molybdenum-Catalyzed Asymmetric Intraannular Ring-Closing Metathesis. *Organometallics* **2015**, *34*, 1197−1202. (i) Hock, A. S.; Schrock, R. R.; Hoveyda, A. H.

Dipyrrolyl Precursors to Bisalkoxide Molybdenum Olefin Metathesis Catalysts. *J. Am. Chem. Soc.* **2006**, *128*, 16373−16375.

(11) Rosenberg, B.; Vancamp, L.; Trosko, J. E.; Mansour, V. H. Platinum Compounds: a New Class of Potent Antitumour Agents. *Nature* **1969**, *222*, 385−386.

(12) Manegold, C.; Gatzemeier, U.; von Pawel, J.; Pirker, R.; Malayeri, R.; Blatter, J.; Krejcy, K. Front-line Treatment of Advanced Non-small-cell Lung Cancer with MTA (LY231514, Pemetrexed Disodium, ALIMTA and Cisplatin: A multicenter phase II Trial. *Ann. Oncol.* **2000**, *11*, 435−440.

(13) Jamieson, E. R.; Lippard, S. J. Structure, Recognition, and Processing of Cisplatin(a) -DNA Adducts. *Chem. Rev.* **1999**, *99*, 2467−2498. (b) Wu, Z.; Liu, Q.; Liang, X.; Yang, X.; Wang, N.; Wang, X.; Sun, H.; Lu, Y.; Guo, Z. Reactivity of Platinum-Based Antitumor Drugs Towards a Met- and His-rich 20mer Peptide Corresponding to the N-terminal Domain of Human Copper Transporter 1. *JBIC, J. Biol. Inorg. Chem.* **2009**, *14*, 1313−1323. (c) Jung, Y.; Lippard, S. J. Direct Cellular Responses to Platinum-Induced DNA Damage. *Chem. Rev.* **2007**, *107*, 1387−1407.

(14) Esteban-Fernandez, D.; Moreno-Gordaliza, E.; Canas, B.; Antonia Palacios, M.; Milagros Gomez-Gomez, M. Analytical methodologies for metallomics studies of antitumor Pt-containing drugs. *Metallomics* **2010**, *2*, 19−38.

(15) Fuertes, M. A.; Alonso, C.; Pérez, J. M. Biochemical Modulation of Cisplatin Mechanisms of Action: Enhancement of Antitumor Activity and Circumvention of Drug Resistance. *Chem. Rev.* **2003**, *103*, 645−662.

(16) Ronconi, L.; Sadler, P. J. Using coordination chemistry to design new medicines. *Coord. Chem. Rev.* **2007**, *251*, 1633−1648.

(17) Rajendiran, V.; Karthik, R.; Palaniandavar, M.; Periasamy, V. S.; Akbarsha, M. A.; Srinag, B. S.; Krishnamurthy, H. Mixed-Ligand Copper(II)-phenolate Complexes: Effect of Coligand on Enhanced DNA and Protein Binding, DNA Cleavage, and Anticancer Activity. *Inorg. Chem.* **2007**, *46*, 8208−8221.

(18) Giannicchi, I.; Brissos, R.; Ramos, D.; Lapuente, J. d.; Lima, J. C.; Cort, A. D.; Rodríguez, L. Substituent Effects on the Biological Properties of Zn-Salophen Complexes. *Inorg. Chem.* **2013**, *52*, 9245−9253.

(19) Bhattacharya, S.; Mandal, S. S. DNA Cleavage by Intercalatable Cobalt−Bispicolylamine Complexes Activated by Visible Light. *Chem. Commun.* **1996**, 1515−1516.

(20) Czlapinski, J. L.; Sheppard, T. L. Nucleic Acid Template-Directed Assembly of Metallosalen−DNA Conjugates. *J. Am. Chem. Soc.* **2001**, *123*, 8618−8619.

(21) Muller, J. G.; Paikoff, S. J.; Rokita, S. E.; Burrows, C. J. DNA Modification Promoted by Water-Soluble Nickel(II) Salen complexes: A switch to DNA alkylation. *J. Inorg. Biochem.* **1994**, *54*, 199−206.

(22) (a) Ansari, K. I.; Grant, J. D.; Kasiri, S.; Woldemariam, G. A.; Shrestha, B.; Mandal, S. S. Manganese(III)-salens induce tumor selective apoptosis in human cells. *J. Inorg. Biochem.* **2009**, *103*, 818−826. (b) Arola-Arnal, A.; Benet-Buchholz, J.; Neidle, S.; Vilar, R. Effects of Metal Coordination Geometry on Stabilization of Human Telomeric Quadruplex DNA by Square-Planar and Square-Pyramidal Metal Complexes. *Inorg. Chem.* **2008**, *47*, 11910−11919. (c) Clever, G. H.; Söltl, Y.; Burks, H.; Spahl, W.; Carell, T. Metal−Salen-Base-Pair Complexes Inside DNA: Complexation Overrides Sequence Information. *Chem. - Eur. J.* **2006**, *12*, 8708−8718. (d) Ansari, K. I.; Grant, J. D.; Woldemariam, G. A.; Kasiri, S.; Mandal, S. S. Iron(III)-salen Complexes with Less DNA cleavage Activity Exhibit More Efficient Apoptosis in MCF7 cells. *Org. Biomol. Chem.* **2009**, *7*, 926−932.

(23) Ansari, K. I.; Kasiri, S.; Grant, J. D.; Mandal, S. S. Apoptosis and Anti-Tumour Activities of Manganese(III)-Salen and -Salphen Complexes. *Dalton Trans.* **2009**, 8525−8531.

(24) Vrdoljak, V.; Đilović, I.; Rubčić, M.; Kraljević Pavelić, S.; Kralj, M.; Matković-Čalogović, D.; Piantanida, I.; Novak, P.; Rožman, A.; Cindrić, M. Synthesis and Characterisation of Thiosemicarbazonato Molybdenum(VI) Complexes and their In Vitro Antitumor Activity. *Eur. J. Med. Chem.* **2010**, *45*, 38−48.

(25) Bandarra, D.; Lopes, M.; Lopes, T.; Almeida, J.; Saraiva, M. S.; Vasconcellos-Dias, M.; Nunes, C. D.; Félix, V.; Brandão, P.; Vaz, P. D.; Meireles, M.; Calhorda. Mo(II) complexes: A New Family of Cytotoxic Agents? *J. Inorg. Biochem.* **2010**, *104*, 1171−1177.

(26) Mrózek, O.; Šebestová, L.; Vinklárek, J.; Řezáčová, M.; Eisner, A.; Růžičková, Z.; Honzíček, J. Highly Water-Soluble Cyclopentadienyl and Indenyl Molybdenum(II) Complexes − Second Generation of Molybdenum-Based Cytotoxic Agents. *Eur. J. Inorg. Chem.* **2016**, *2016*, 519−529.

(27) Harding, M. M.; Mokdsi, G.; Mackay, J. P.; Prodigalidad, M.; Lucas, S. W. Interactions of the Antitumor Agent Molybdocene Dichloride with Oligonucleotides. *Inorg. Chem.* **1998**, *37*, 2432−2437.

(28) Narváez-Pita, X.; Ortega-Zuniga, C.; Acevedo-Morantes, C. Y.; Pastrana, B.; Olivero-Verbel, J.; Maldonado-Rojas, W.; Ramírez-Vick, J. E.; Meléndez, E. Water Soluble Molybdenocene Complexes: Synthesis, Cytotoxic Activity and Binding Studies to Ubiquitin by Fluorescence Spectroscopy, Circular Dichroism and Molecular Modeling. *J. Inorg. Biochem.* **2014**, *132*, 77−91.

(29) Gleeson, B.; Claffey, J.; Deally, A.; Hogan, M.; Méndez, L. M. M.; Müller-Bunz, H.; Patil, S.; Tacke, M. Novel Benzyl-Substituted Molybdocene Anticancer Drugs. *Inorg. Chim. Acta* **2010**, *363*, 1831−1836.

(30) Harding, M. M.; Harden, G. J.; Field, L. D. A ^{31}P NMR Study of the Interaction of the Antitumor Active Metallocene Cp_2MoCl_2 with calf thymus DNA. *FEBS Lett.* **1993**, *322*, 291−294.

(31) Feng, J.; Lu, X.-m.; Wang, G.; Du, S.-z.; Cheng, Y.-f. The Syntheses and Characterizations of Molybdenum(VI) complexes with Catechol and 2,3-Dihydroxynaphthalene, and the Structure−Effect Relationship in their *in vitro* Anticancer Activities. *Dalton Trans.* **2012**, *41*, 8697−8702.

(32) Cindrić, M.; Novak, T. K.; Kraljević, S.; Kralj, M.; Kamenar, B. Structural and Antitumor Activity Study of γ-Octamolybdates Containing Aminoacids and Peptides. *Inorg. Chim. Acta* **2006**, *359*, 1673−1680.

(33) Zhang, K.; Cui, S.; Wang, J.; Wang, X.; Li, R. Study on Antitumor Activity of Metal-Based Diketone Complexes. *Med. Chem. Res.* **2012**, *21*, 1071−1076.

(34) Saraiva, M. S.; Quintal, S.; Portugal, F. C. M.; Lopes, T. A.; Félix, V.; Nogueira, J. M. F.; Meireles, M.; Drew, M. G. B.; Calhorda, M. J. Nitrogen Donor Ligands Bearing N−H Groups: Effect on Catalytic and Cytotoxic Activity of Molybdenum η³-Allyldicarbonyl Complexes. *J. Organomet. Chem.* **2008**, *693*, 3411−3418.

(35) (a) Rao, N. S.; Mishra, D. D.; Maurya, R. C.; Rao, N. N. Synthesis and Characterisation of Some Novel CIS-Dioxo-Molybdenum (VI) Complexes of Schiff Bases Derived from Salicylaldehyde. *Synth. React. Inorg. Met.-Org. Chem.* **1995**, *25*, 437−449. (b) Hill, W. E.; Atabay, N.; McAuliffe, C. A.; McCullough, F. P.; Razzoki, S. M. The coordination chemistry of Molybdenum and Tungsten. Part XIV. Dioxomolybdenum(VI) Complexes of Bidentate, Tridentate, and Tetradentate Schiff Bases Containing Oxygen, Nitrogen and Sulphur Donors. *Inorg. Chim. Acta* **1979**, *35*, 35−41. (c) El-Medani, S. M.; Ali, O. A. M.; Ramadan, R. M. Photochemical Reactions of Group 6 Metal Carbonyls with N-Salicylidene-2-Hydroxyaniline and Bis-(salicylaldehyde)phenylenediimine. *J. Mol. Struct.* **2005**, *738*, 171−177. (d) Tarafder, M. T. H.; Khan, A. R. Peroxo Complexes of Zirconium(IV), Thorium(IV), Molybdenum(VI), Tungsten(VI) and Uranium(VI) Containing Two Quadridentate ONNO Schiff Bases. *Polyhedron* **1991**, *10*, 819−822.

(36) (a) Bruno, S. M.; Balula, S. S.; Valente, A. A.; Almeida Paz, F. A.; Pillinger, M.; Sousa, C.; Klinowski, J.; Freire, C.; Ribeiro-Claro, P.; Gonçalves, I. S. Synthesis and Catalytic Properties in Olefin Epoxidation of Dioxomolybdenum(VI) Complexes Bearing a Bidentate or Tetradentate Salen-Type Ligand. *J. Mol. Catal. A: Chem.* **2007**, *270*, 185−194. (b) Schilf, W.; Kamieński, B.; Rozwadowski, Z.; Ambroziak, K.; Bieg, B.; Dziembowska, T. Solid State ^{15}N and ^{13}C NMR Study of Dioxomolybdenum (VI) Complexes of Schiff Bases Derived From Trans-1,2-Cyclohexanediamine. *J. Mol. Struct.* **2004**, *700*, 61−65. (c) Cameron, J. H.; McEwan, J. A. Tridentate Coordination of Dioxomolybdenum(VI) with Some

Potentially Quinquedentate (N_2O_3) Schiff Base Ligands. *Inorg. Chim. Acta* **1993**, *211*, 111−116.

(37) (a) Schley, M.; Fritzsche, S.; Lonnecke, P.; Hey-Hawkins, E. Soluble Monometallic Salen Complexes Derived from O-Functionalised Diamines as Metalloligands for the Synthesis of Heterobimetallic Complexes. *Dalton Trans.* **2010**, *39*, 4090−4106. (b) Judmaier, M. E.; Holzer, C.; Volpe, M.; Mösch-Zanetti, N. C. Molybdenum(VI) Dioxo Complexes Employing Schiff Base Ligands with an Intramolecular Donor for Highly Selective Olefin Epoxidation. *Inorg. Chem.* **2012**, *51*, 9956−9966. (c) Pandhare, S. L.; Jadhao, R. R.; Puranik, V. G.; Joshi, P. V.; Capet, F.; Dongare, M. K.; Umbarkar, S. B.; Michon, C.; Agbossou-Niedercorn, F. Molybdenum(VI) Dioxo Complexes for the Epoxidation of Allylic Alcohols and Olefins. *J. Organomet. Chem.* **2014**, *772−773*, 271−279.

(38) (a) Dash, S. P.; Pasayat, S.; Bhakat, S.; Roy, S.; Dinda, R.; Tiekink, E. R. T.; Mukhopadhyay, S.; Bhutia, S. K.; Hardikar, M. R.; Joshi, B. N.; Patil, Y. P.; Nethaji, M. Highly Stable Hexacoordinated Nonoxidovanadium(IV) Complexes of Sterically Constrained Ligands: Syntheses, Structure, and Study of Antiproliferative and Insulin Mimetic Activity. *Inorg. Chem.* **2013**, *52*, 14096−14107. (b) Pasayat, S.; Dash, S. P.; Majumder, S.; Dinda, R.; Sinn, E.; Stoeckli-Evans, H.; Mukhopadhyay, S.; Bhutia, S. K.; Mitra, P. Synthesis, Structure, Characterization and Study of Antiproliferative Activity of Dimeric and Tetrameric Oxidomolybdenum(VI) Complexes of N,N′-disalicyloyl-hydrazine. *Polyhedron* **2014**, *80*, 198−205. (c) Saswati; Chakraborty, A.; Dash, S. P.; Panda, A. K.; Acharyya, R.; Biswas, A.; Mukhopadhyay, S.; Bhutia, S. K.; Crochet, A.; Patil, Y. P.; Nethaji, M.; Dinda, R. Synthesis, X-ray Structure and *in vitro* Cytotoxicity Studies of Cu(I/II) Complexes of Thiosemicarbazone: Special Emphasis on their Interactions with DNA. *Dalton Trans.* **2015**, *44*, 6140−6157. (d) Dash, S. P.; Panda, A. K.; Pasayat, S.; Majumder, S.; Biswas, A.; Kaminsky, W.; Mukhopadhyay, S.; Bhutia, S. K.; Dinda, R. Evaluation of the Cell Cytotoxicity and DNA/BSA Binding and Cleavage Activity of some Dioxidovanadium(V) Complexes Containing Aroylhydrazones. *J. Inorg. Biochem.* **2015**, *144*, 1−12. (e) Dash, S. P.; Panda, A. K.; Pasayat, S.; Dinda, R.; Biswas, A.; Tiekink, E. R. T.; Mukhopadhyay, S.; Bhutia, S. K.; Kaminsky, W.; Sinn, E. Oxidovanadium(V) Complexes of Aroylhydrazones Incorporating Heterocycles: Synthesis, Characterization and Study of DNA Binding, Photoinduced DNA Cleavage and Cytotoxic Activities. *RSC Adv.* **2015**, *5*, 51852−51867. (f) Dash, S. P.; Panda, A. K.; Pasayat, S.; Dinda, R.; Biswas, A.; Tiekink, E. R. T.; Patil, Y. P.; Nethaji, M.; Kaminsky, W.; Mukhopadhyay, S.; Bhutia, S. K. Syntheses and Structural Investigation of Some Alkali Metal Ion-Mediated $L^V VO^{2−}$ ($L^{2−}$ = tridentate ONO ligands) Species: DNA Binding, Photoinduced DNA Cleavage and Cytotoxic Activities. *Dalton Trans.* **2014**, *43*, 10139−10156. (g) Dash, S. P.; Panda, A. K.; Dhaka, S.; Pasayat, S.; Biswas, A.; Maurya, M. R.; Majhi, P. K.; Crochet, A.; Dinda, R. A Study of DNA/BSA Interaction and Catalytic Potential of Oxidovanadium(V) Complexes with ONO Donor ligands. *Dalton Trans.* **2016**, *45*, 18292−18307.

(39) Mandal, S.; Mandal, S.; Seth, D. K.; Mukhopadhyay, B.; Gupta, P. Ruthenium and Osmium Complexes of Novel Carbohydrate Derived Salen Ligands: Synthesis, Characterization and *in situ* Ligand Reduction. *Inorg. Chim. Acta* **2013**, *398*, 83−88.

(40) (a) Minato, M.; Fujiwara, Y.; Koga, M.; Matsumoto, N.; Kurishima, S.; Natori, M.; Sekizuka, N.; Yoshioka, K.-i.; Ito, T. Reductions of C=O and C=N groups With the Systems Composed of $(\eta^5-C_5H_5)_2MoH_2$ and Acids. *J. Organomet. Chem.* **1998**, *569*, 139−145.

(41) (a) Maurya, M. R.; Kumar, A.; Ebel, M.; Rehder, D. Synthesis, Characterization, Reactivity, and Catalytic Potential of Model Vanadium(IV, V) Complexes with Benzimidazole-Derived ONN Donor Ligands. *Inorg. Chem.* **2006**, *45*, 5924−5937. (b) Bertini, S.; Coletti, A.; Floris, B.; Conte, V.; Galloni, P. Investigation of VO−Salophen Complexes Electronic structure. *J. Inorg. Biochem.* **2015**, *147*, 44−53. (c) Tzubery, A.; Tshuva, E. Y. Trans Titanium(IV) Complexes of Salen Ligands Exhibit High Antitumor Activity. *Inorg. Chem.* **2011**, *50*, 7946−7948. (d) Castro-Osma, J. A.; Lamb, K. J.; North, M. Cr(salophen) Complex Catalyzed Cyclic Carbonate Synthesis at

Ambient Temperature And Pressure. *ACS Catal.* **2016**, *6*, 5012−5025. (e) Bhowmik, P.; Nayek, H. P.; Corbella, M.; Aliaga-Alcalde, N.; Chattopadhyay, S. Control of Molecular Architecture by Steric Factors: Mononuclear vs Polynuclear Manganese(III) Compounds with Tetradentate N_2O_2 Donor Schiff Bases. *Dalton Trans.* **2011**, *40*, 7916−7926. (f) Jana, S.; Chatterjee, S.; Chattopadhyay, S. Syntheses, Characterization and X-ray Crystal Structures of Hexa-Coordinated Monomeric and Oxo-Bridged Dimeric Fe(III) Compounds with Salen-type Schiff Bases. *Polyhedron* **2012**, *48*, 189−198. (g) Amirnasr, M.; Schenk, K. J.; Gorji, A.; Vafazadeh, R. Synthesis and Spectroscopic Characterization of $[Co^{III}(salophen)(amine)_2]ClO_4$ (amine = morpholine, pyrrolidine, and piperidine) complexes. The crystal structures of $[Co^{III}(salophen)(morpholine)_2]ClO_4$ and $[Co^{III}(salophen)-(pyrrolidine)_2]ClO_4$. *Polyhedron* **2001**, *20*, 695−702. (h) de Bellefeuille, D.; Askari, M. S.; Lassalle-Kaiser, B.; Journaux, Y.; Aukauloo, A.; Orio, M.; Thomas, F.; Ottenwaelder, X. Reversible Double Oxidation and Protonation of the Non-Innocent Bridge in a Nickel(II) Salophen Complex. *Inorg. Chem.* **2012**, *51*, 12796−12804. (i) de Bellefeuille, D.; Orio, M.; Barra, A.-L.; Aukauloo, A.; Journaux, Y.; Philouze, C.; Ottenwaelder, X.; Thomas, F. Redox Noninnocence of the Bridge in Copper(II) Salophen and Bis(oxamato) Complexes. *Inorg. Chem.* **2015**, *54*, 9013−9026. (j) Escudero-Adán, E. C.; Benet-Buchholz, J.; Kleij, A. W. Expedient Method for the Transmetalation of Zn(II)-Centered Salphen Complexes. *Inorg. Chem.* **2007**, *46*, 7265−7267. (k) Wong, T.-W.; Lau, T.-C.; Wong, W.-T. Osmium(VI) Nitrido and Osmium(IV) Phosphoraniminato Complexes Containing Schiff Base Ligands. *Inorg. Chem.* **1999**, *38*, 6181−6186. (l) Proetto, M. T.; Liu, W.; Molchanov, A.; Sheldrick, W. S.; Hagenbach, A.; Abram, U.; Gust, R. Synthesis, Characterization, and in vitro Antiproliferative Activity of [Salophene]platinum(II) Complexes. *ChemMedChem* **2014**, *9*, 1176−1187.

(42) Chen, G. J. J.; McDonald, J. W.; Newton, W. E. Synthesis of Molybdenum(IV) and Molybdenum(V) Complexes using Oxo Abstraction by Phosphines. Mechanistic Implications. *Inorg. Chem.* **1976**, *15*, 2612−2615.

(43) Choudhary, N. F.; Connelly, N. G.; Hitchcock, P. B.; Leigh, G. J. New Compounds of Tetradentate Schiff Bases with Vanadium(IV) and Vanadium(V). *J. Chem. Soc., Dalton Trans.* **1999**, 4437−4446.

(44) Ding, L.; Jin, W.; Chu, Z.; Chen, L.; Lü, X.; Yuan, G.; Song, J.; Fan, D.; Bao, F. Bulk Solvent-Free Melt Ring-Opening Polymerization (ROP) of L-Lactide Catalyzed by Ni(II) and Ni(II)−Ln(III) Complexes Based on the Acyclic Salen-Type Schiff-Base Ligand. *Inorg. Chem. Commun.* **2011**, *14*, 1274−1278.

(45) (a) Bruker *APEX2 (version 2.1-4); SAINT (version 7.34A); SADABS (version 2007/4)*; BrukerAXS Inc: Madison, WI, USA, 2007. (b) Sheldrick, G. M.; *SHELXS-97, Program for Crystal Structure Determination*; Universität Göttingen: Göttingen, Germany, 1997.

(46) (a) Sheldrick, G. M. *SHELXL-97, Program for Refinement of Crystal Structures*; Universität Göttingen: Göttingen, Germany, 1997. (b) Mackay, S.; Edwards, C.; Henderson, A.; Gilmore, C.; Stewart, N.; Shankland, K.; Donald, A. *MaXus: A computer program for the solution and refinement of crystal structures from diffraction data*; University of Glasgow: Glasgow, Scotland, 1997.

(47) (a) Kumar, P.; Gorai, S.; Kumar Santra, M.; Mondal, B.; Manna, D. DNA Binding, Nuclease Activity and Cytotoxicity Studies of Cu(II) Complexes of Tridentate Ligands. *Dalton Trans.* **2012**, *41*, 7573−7581. (b) Suzuki, T.; Fujikura, K.; Higashiyama, T.; Takata, K. DNA Staining for Fluorescence and Laser Confocal Microscopy. *J. Histochem. Cytochem.* **1997**, *45*, 49−53. (c) Pasayat, S.; Böhme, M.; Dhaka, S.; Dash, S. P.; Majumder, S.; Maurya, M. R.; Plass, W.; Kaminsky, W.; Dinda, R. Synthesis, Theoretical Study and Catalytic Application of Oxidometal (Mo or V) Complexes: Unexpected Coordination Due to Ligand Rearrangement through Metal-Mediated C−C Bond Formation. *Eur. J. Inorg. Chem.* **2016**, *2016*, 1604−1618. (d) Brondino, C. D.; Rivas, M. G.; Romão, M. J.; Moura, J. J. G.; Moura, I. Structural and Electron Paramagnetic Resonance (EPR) Studies of Mononuclear Molybdenum Enzymes from Sulfate-Reducing Bacteria. *Acc. Chem. Res.* **2006**, *39*, 788−796. (e) Yang, Z.; Gould, E. S. Reactions of

molybdenum(VI) with metal ion reductants. *Dalton Trans.* **2006**, 3427−3430.

(48) (a) Nagy, E. M.; Pettenuzzo, A.; Boscutti, G.; Marchiò, L.; Dalla Via, L.; Fregona, D. Ruthenium(II/III)-Based Compounds with Encouraging Antiproliferative Activity against Non-small-Cell Lung Cancer. *Chem. - Eur. J.* **2012**, *18*, 14464−14472. (b) Melby, L. R. Crystalline Molybdenum(V)-Histidine Complex. *Inorg. Chem.* **1969**, *8*, 1539−1540. (c) Spence, J. T.; Lee, J. Y. Histidine Complexes of Molybdenum(V) and Molybdenum(VI). *Inorg. Chem.* **1965**, *4*, 385−388.

(49) (a) Dinda, R.; Sengupta, P.; Ghosh, S.; Sheldrick, W. S. Synthesis, Structure, and Reactivity of a New Mononuclear Molybdenum(VI) Complex Resembling the Active Center of Molybdenum Oxotransferases. *Eur. J. Inorg. Chem.* **2003**, *2003*, 363−369. (b) Dinda, R.; Ghosh, S.; Falvello, L. R.; Tomás, M.; Mak, T. C. W. Synthesis, Structure, and Reactivity of Some New Dipyridyl and Diamine-Bridged Dinuclear Oxomolybdenum(VI) Complexes. *Polyhedron* **2006**, *25*, 2375−2382. (c) Dinda, R.; Sengupta, P.; Ghosh, S.; Mayer-Figge, H.; Sheldrick, W. S. A family of Mononuclear Molybdenum-(VI), and -(IV) Oxo Complexes with a Tridentate (ONO) Ligand. *J. Chem. Soc., Dalton Trans.* **2002**, 4434−4439. (d) Huang, T. J.; Haight, G. P., Jr. Paramagnetic Monomeric Molybdenum (V) − Cysteine Complex as a Model for Molybdenum-Enzyme Interaction. *J. Am. Chem. Soc.* **1970**, *92*, 2336−2342. (e) Chaudhury, M. Chemistry of molybdenum. 3. Synthesis, Characterization, And Electrochemical Studies Of Monomeric Oxodihalogenomolybdenum(VI), -Molybdenum(V), And -Molybdenum(IV) Complexes Of 2-Aminocyclopent-1-Ene-1-Dithiocarboxylic Acid. *Inorg. Chem.* **1984**, *23*, 4434−4439. (f) Basu, P.; Nemykin, V. N.; Sengar, R. S. Syntheses, Spectroscopy, and Redox Chemistry of Encapsulated Oxo−Mo(V) Centers: Implications for Pyranopterin-Containing Molybdoenzymes. *Inorg. Chem.* **2003**, *42*, 7489−7501.

(50) (a) Bermejo, M. R.; Fernández, M. I.; González-Noya, A. M.; Maneiro, M.; Pedrido, R.; Rodríguez, M. J.; García-Monteagudo, J. C.; Donnadieu, B. Novel Peroxidase Mimics: μ-Aqua Manganese−Schiff Base Dimers. *J. Inorg. Biochem.* **2006**, *100*, 1470−1478. (b) Bermejo, M. R.; Fernández, M. I.; Gómez-Fórneas, E.; González-Noya, A.; Maneiro, M.; Pedrido, R.; Rodríguez, M. J. Self-Assembly of Dimeric Mn^{III}−Schiff-Base Complexes Tuned by Perchlorate Anions. *Eur. J. Inorg. Chem.* **2007**, *2007*, 3789−3797.

(51) (a) Bray, R. C. EPR of Molybdenum-Containing Enzymes. In *Biological Magnetic Resonance*; Berliner, L. J., Reuben, J., Ed.; Plenum Press: New York, 1980; *Vol. 2*, 45−84. (b) Hanson, G. R.; Noble, C. J.; Benson, S. Molecular Sophe: An Integrated Approach to the Structural Characterization of Metalloproteins: The Next Generation of Computer Simulation Software. In *High Resolution EPR: Applications to Metalloenzymes and Metals in Medicine*; Berliner, L., Hanson, G., Ed.; Springer: New York, New York, 2009, 105−173. (c) Chang, C. S. J.; Collison, D.; Mabbs, F. E.; Enemark, J. H. Synthesis and Characterization of Mononuclear Oxomolybdenum(V) Complexes with Aliphatic Diolato, Dithiolato, or Alkoxo Ligands: Effect of Chelate Ring Size on the Properties of the Metal Center. *Inorg. Chem.* **1990**, *29*, 2261−2267.

(52) (a) Bose, M.; Moula, G.; Sarkar, S. Mono-(maleonitriledithiolene) molybdenum(IV) and Bis(μ-sulfido)-Bridged Dimolybdenum(V) Complexes with Mo = S Moiety. *Chem. Biodiversity* **2012**, *9*, 1867−1879. (b) Modec, B.; Šala, M.; Clérac, R. Clérac Pyrazine-Assisted Dimerization of Molybdenum(V): Synthesis and Structural Characterization of Novel Dinuclear and Tetranuclear Complexes. *Eur. J. Inorg. Chem.* **2010**, *2010*, 542−553.

(53) (a) Bhattacharya, K.; Abtab, S. M. T.; Majee, M. C.; Endo, A.; Chaudhury, M. Targeted Synthesis of Heterobimetallic Compounds Containing a Discrete Vanadium(V)−μ-Oxygen−Iron(III) Core. *Inorg. Chem.* **2014**, *53*, 8287−8297. (b) Taylor, R. D.; Street, J. P.; Minelli, M.; Spence, J. T. Electrochemistry Of Monomeric Molybdenum(V)-Oxo Complexes In Dimethylformamide. *Inorg. Chem.* **1978**, *17*, 3207−3211. (c) Conry, R. R.; Tipton, A. A. A mononuclear molybdenum(V) mono-oxo biphenyl-2,2′-dithiolate

complex in which the metal resides within a cleft formed by the ligands and that exhibits N-H•••S hydrogen bonding in the solid state. *JBIC, J. Biol. Inorg. Chem.* **2001**, *6*, 359−366. (d) Thomas, F.; Jarjayes, O.; Duboc, C.; Philouze, C.; Saint-Aman, E.; Pierre, J.-L. Intramolecularly hydrogen-bonded *versus* copper(II) coordinated mono- and bis-phenoxyl radicals. *Dalton Trans.* **2004**, 2662−2669.

(54) Parimala, S.; Selvam, P. Crystal structure of aquadioxido-(2-{[(2-oxidoethyl)imino]methyl}phenolato-*κ*³ O,N,O′)molybdenum-(VI). *Acta Crystallogr. Sect. E* **2015**, *71*, m35−m36.

(55) (a) Hille, R. The Mononuclear Molybdenum Enzymes. *Chem. Rev.* **1996**, *96*, 2757−2816. (b) Romão, M. J.; Archer, M.; Moura, I.; Moura, J. J. G.; LeGall, J.; Engh, R.; Schneider, M.; Hof, P.; Huber, R. Crystal Structure of the Xanthine Oxidase-Related Aldehyde Oxido-Reductase from D. gigas. *Science* **1995**, *270*, 1170−1176.

(56) Modec, B.; Brenčič, J. V.; Finn, R. C.; Rarig, R. S.; Zubieta, J. Structural Isomerism Among Octanuclear Oxomolybdenum(V) Coordination Compounds with Pyridines. Two Isomers of [Mo₈O₁₆(OCH₃)₈(R−Py)₄]. *Inorg. Chim. Acta* **2001**, *322*, 113−119.

(57) (a) Pasayat, S.; Dash, S. P.; Saswati; Majhi, P. K.; Patil, Y. P.; Nethaji, M.; Dash, H. R.; Das, S.; Dinda, R. Mixed-Ligand Aroylhydrazone Complexes of Molybdenum: Synthesis, Structure and Biological Activity. *Polyhedron* **2012**, *38*, 198−204. (b) Pasayat, S.; Dash, S. P.; Roy, S.; Dinda, R.; Dhaka, S.; Maurya, M. R.; Kaminsky, W.; Patil, Y. P.; Nethaji, M. Synthesis, Structural Studies and Catalytic Activity of Dioxidomolybdenum(VI) Complexes with Aroylhydra-zones of Naphthol-Derivative. *Polyhedron* **2014**, *67*, 1−10.

(58) (a) Subramanian, P.; Spence, J. T.; Ortega, R.; Enemark, J. H. Molybdenum(VI)-dioxo Complexes with Sterically Bulky Ligands. *Inorg. Chem.* **1984**, *23*, 2564−2572. (b) Dupe, A.; Judmaier, M. E.; Belaj, F.; Zangger, K.; Mosch-Zanetti, N. C. Activation of Molecular Oxygen by a Molybdenum Complex for Catalytic Oxidation. *Dalton Trans.* **2015**, *44*, 20514−20522. (c) Yüksektepe Ataol, Ç.; Şenyüz, N.; Bat, H. Spectroscopy and X-ray studies of {{6,6′-dimethoxy-2,2′-[ethane-1,2-diyl-bis-(nitrilomethylidyne)]diphenolato}(aqua)-dioxouranium(VI)} dehydrate. *Russ. J. Coord. Chem.* **2014**, *40*, 671−675.

(59) Arjmand, F.; Mohani, B.; Ahmad, S. Synthesis, Antibacterial, Antifungal Activity and Interaction of CT-DNA with a New Benzimidazole Derived Cu(II) Complex. *Eur. J. Med. Chem.* **2005**, *40*, 1103−1110.

(60) Rajendiran, V.; Murali, M.; Suresh, E.; Sinha, S.; Somasundaram, K.; Palaniandavar, M. Mixed Ligand Ruthenium(II) Complexes of Bis(pyrid-2-yl)-/Bis(Benzimidazol-2-yl)-Dithioether and Diimines: Study of Non-Covalent DNA Binding and Cytotoxicity. *Dalton Trans.* **2008**, 148−163.

(61) (a) Arjmand, F.; Aziz, M. Synthesis and Characterization of Dinuclear Macrocyclic Cobalt(II), Copper(II) and Zinc(II) Com-plexes Derived from 2,2,2′,2′-S,S[Bis(Bis-N,N-2-Thiobenzimidazoly-loxalato-1,2-Ethane)]: DNA Binding and Cleavage Studies. *Eur. J. Med. Chem.* **2009**, *44*, 834−844. (b) Neidle, S. DNA minor-groove recognition by small molecules. *Nat. Prod. Rep.* **2001**, *18*, 291−309. (c) Bindu, P. J.; Mahadevan, K. M.; Naik, T. R. R.; Harish, B. G. Synthesis, DNA binding, docking and photocleavage studies of quinolinyl chalcones. *MedChemComm* **2014**, *5*, 1708−1717. (d) Jeya-lakshmi, K.; Arun, Y.; Bhuvanesh, N. S. P.; Perumal, P. T.; Sreekanth, A.; Karvembu, R. DNA/protein binding, DNA cleavage, cytotoxicity, superoxide radical scavenging and molecular docking studies of copper(II) complexes containing N-benzyl-N′-aryl-N″-benzoylguani-dine ligands. *Inorg. Chem. Front.* **2015**, *2*, 780−798.

(62) (a) An, Y.; Liu, S.-D.; Deng, S.-Y.; Ji, L.-N.; Mao, Z.-W. Cleavage of Double-Strand DNA by Linear and Triangular Trinuclear Copper Complexes. *J. Inorg. Biochem.* **2006**, *100*, 1586−1593. (b) Banerjee, S.; Hussain, A.; Prasad, P.; Khan, I.; Banik, B.; Kondaiah, P.; Chakravarty, A. R. Photocytotoxic Oxidovanadium(IV) Complexes of Polypyridyl Ligands Showing DNA-Cleavage Activity in Near-IR Light. *Eur. J. Inorg. Chem.* **2012**, *2012*, 3899−3908.

(63) Poklar, N.; Pilch, D. S.; Lippard, S. J.; Redding, E. A.; Dunham, S. U.; Breslauer, K. J. Influence of Cisplatin Intrastrand Crosslinking on the Conformation, Thermal Stability, and Energetics of a 20-mer DNA Duplex. *Proc. Natl. Acad. Sci. U. S. A.* **1996**, *93*, 7606−7611.

(64) Li, L.; Guo, Q.; Dong, J.; Xu, T.; Li, J. DNA Binding, DNA Cleavage and BSA Interaction of a Mixed-Ligand Copper(II) Complex with Taurine Schiff Base and 1,10-Phenanthroline. *J. Photochem. Photobiol., B* **2013**, *125*, 56−62.

(65) (a) Dai, W.-M.; Lai, K. W.; Wu, A.; Hamaguchi, W.; Lee, M. Y. H.; Zhou, L.; Ishii, A.; Nishimoto, S.-i. DNA Cleavage Potency, Cytotoxicity, and Mechanism of Action of a Novel Class of Enediyne Prodrugs. *J. Med. Chem.* **2002**, *45*, 758−761. (b) Pardhi, M.; Verma, B.; Thakur, Y.; Khilari, R.; Tripathi, M.; Pande, R. *in vitro* Screening of N-Naphthylhydroxamic Acids as DNA Binding Agents. *Asian J. Chem.* **2016**, *28*, 2605−2612. (c) Pages, B. J.; Ang, D. L.; Wright, E. P.; Aldrich-Wright, J. R. Metal Complex Interactions with DNA. *Dalton Trans.* **2015**, *44*, 3505−3526.

(66) (a) Kim, J. S.; Gatto, B.; Yu, C.; Liu, A.; Liu, L. F.; LaVoie, E. J. Substituted 2,5′-Bi-1H-benzimidazoles: Topoisomerase I Inhibition and Cytotoxicity. *J. Med. Chem.* **1996**, *39*, 992−998. (b) Sasmal, P. K.; Saha, S.; Majumdar, R.; De, S.; Dighe, R. R.; Chakravarty, A. R. Oxovanadium(IV) Complexes of Phenanthroline Bases: the Dipyr-idophenazine Complex as a Near-IR Photocytotoxic Agent. *Dalton Trans.* **2010**, *39*, 2147−2158.

(67) (a) Efthimiadou, E. K.; Karaliota, A.; Psomas, G. Mononuclear Dioxomolybdenum(VI) Complexes with the Quinolones Enrofloxacin and Sparfloxacin: Synthesis, Structure, Antibacterial Activity and Interaction with DNA. *Polyhedron* **2008**, *27*, 349−356. (b) Hussein, M. A.; Guan, T. S.; Haque, R. A.; Ahamed, M. B. K.; Majid, A. M. S. A. Synthesis and Characterization of Thiosemicarbazonato Molybdenum-(VI) Complexes: In vitro DNA Binding, Cleavage, and Antitumor Activities. *Polyhedron* **2015**, *85*, 93−103. (c) Selim, M.; Saha, A.; Mukherjea, K. K. Synthesis, characterization, and DNA binding of the biologically relevant novel cationic molybdenum(VI)−glutathione complex [Mo(GS)(Cl)(H₂O)]Cl₂. *Monatsh. Chem.* **2012**, *143*, 227−233. (d) Ahmadi, S. M.; Dehghan, G.; Hosseinpourfeizi, M. A.; Dolatabadi, J. E. N.; Kashanian, S. Preparation, Characterization, and DNA Binding Studies of Water-Soluble Quercetin−Molybdenum(VI) Complex. *DNA Cell Biol.* **2011**, *30*, 517−523. (e) Anbu, S.; Kandaswamy, M. Electrochemical, Magnetic, Catalytic, DNA Binding and Cleavage Studies of New Mono and Binuclear Copper(II) Complexes. *Polyhedron* **2011**, *30*, 123−131. (f) Selvarani, V.; Annaraj, B.; Neelakantan, M. A.; Sundaramoorthy, S.; Velmurugan, D. Synthesis, Characterization and Crystal Structures of Copper(II) and Nickel(II) Complexes of Propargyl Arm Containing N₂O₂ Ligands: Antimicrobial Activity and DNA Binding. *Polyhedron* **2013**, *54*, 74−83. (g) Arun, T.; Packianathan, S.; Malarvizhi, M.; Antony, R.; Raman, N. Bio-Relevant Complexes of Novel N₂O₂ Type Heterocyclic ligand: Synthesis, Structural Elucidation, Biological Evaluation and Docking Studies. *J. Photochem. Photobiol, B* **2015**, *149*, 93−102. (h) Mandegani, Z.; Asadi, Z.; Asadi, M.; Karbalaei-Heidari, H. R.; Rastegari, B. Synthesis, Characterization, DNA Binding, Cleavage Activity, Cytotoxicity and Molecular Docking of New Nano Water-Soluble [M(5-CH₂PPh₃-3,4-salpyr)](ClO₄)₂ (M = Ni, Zn) Complexes. *Dalton Trans.* **2016**, *45*, 6592−6611. (i) Kar, S.; Sengupta, D.; Deb, M.; Shilpi, A.; Parbin, S.; Rath, S. K.; Pradhan, N.; Rakshit, M.; Patra, S. K. Expression profiling of DNA methylation-mediated epigenetic gene-silencing factors in breast cancer. *Clin. Epigenet.* **2014**, *6*, 20. (j) Deb, M.; Sengupta, D.; Kar, S.; Rath, S. K.; Roy, S.; Das, G.; Patra, S. K. Epigenetic drift towards histone modifications regulates CAV1 gene expression in colon cancer. *Gene* **2016**, *581*, 75−84.

(68) (a) Zhang, L.; Ren, W.; Wang, X.; Zhang, J.; Liu, J.; Zhao, L.; Zhang, X. Discovery of Novel Polycyclic Spiro-Fused Carbocyclicox-indole-Based Anticancer Agents. *Eur. J. Med. Chem.* **2017**, *126*, 1071−1082. (b) Jung, H.; Dubey, A.; Koo, H. J.; Vajpayee, V.; Cook, T. R.; Kim, H.; Kang, S. C.; Stang, P. J.; Chi, Ki-W. Self-Assembly of Ambidentate Pyridyl-Carboxylate Ligands with Octahedral Ruthenium Metal Centers: Self-Selection for a Single-Linkage Isomer and Anticancer-Potency Studies. *Chem. - Eur. J.* **2013**, *19*, 6709−6717. (c) Ramadan, A. M. Structural and Biological Aspects of Copper (II)

Complexes with 2-Methyl-3-Amino-(3−H)-Quinazolin-4-one. *J. Inorg. Biochem.* **1997**, *65*, 183−189.

(69) Avaji, P. G.; Kumar, C. H. V.; Patil, S. A.; Shivananda, K. N.; Nagaraju, C. Synthesis, Spectral Characterization, In-Vitro Micro-biological Evaluation and Cytotoxic Activities of Novel Macrocyclic Bis Hydrazone. *Eur. J. Med. Chem.* **2009**, *44*, 3552−3559.

(70) Rosu, T.; Pahontu, E.; Pasculescu, S.; Georgescu, R.; Stanica, N.; Curaj, A.; Popescu, A.; Leabu, M. Synthesis, Characterization Antibacterial and Antiproliferative Activity of Novel Cu(II) and Pd(II) Complexes with 2-hydroxy-8-R-tricyclo[7.3.1.0.^{2,7}]Tridecane-13-one Thiosemicarbazone. *Eur. J. Med. Chem.* **2010**, *45*, 1627−1634.

(71) Thomadaki, H.; Karaliota, A.; Litos, C.; Scorilas, A. Enhanced Antileukemic Activity of the Novel Complex 2,5-Dihydroxybenzoate Molybdenum(VI) Against 2,5-Dihydroxybenzoate, Polyoxometalate of Mo(VI), and Tetraphenylphosphonium in the Human HL-60 and K562 Leukemic Cell Lines. *J. Med. Chem.* **2007**, *50*, 1316−1321.

(72) (a) Zhang, G.; Ta, C.; Cheng, S.-Y.; Golen, J. A.; Rheingold, A. L. Clicking Thiourea into a Salen Scaffold: Structures and Cytotoxicity of Cobalt(II) and Nickel(II) Complexes. *Inorg. Chem. Commun.* **2014**, *48*, 127−130. (b) Terenzi, A.; Lotsch, D.; van Schoonhoven, S.; Roller, A.; Kowol, C. R.; Berger, W.; Keppler, B. K.; Barone, G. Another step toward DNA selective targeting: NiII and CuII complexes of a Schiff base ligand able to bind gene promoter G-quadruplexes. *Dalton Trans.* **2016**, *45*, 7758−7767. (c) Herchel, R.; Sindelar, Z.; Travnicek, Z.; Zboril, R.; Vanco, J. Novel 1D Chain Fe(III)-Salen-like Complexes Involving Anionic Heterocyclic N-Donor Ligands. Synthesis, X-ray Structure, Magnetic, 57Fe Mössbauer, and Biological Activity Studies. *Dalton Trans.* **2009**, 9870−9880. (d) Tzubery, A.; Tshuva, E. Y. Cytotoxicity and Hydrolysis of trans-Ti(IV) Complexes of Salen Ligands: Structure−Activity Relationship Studies. *Inorg. Chem.* **2012**, *51*, 1796−1804.

(73) Singh, N.; Ranjan, V.; Zaidi, D.; Shyam, H.; Singh, A.; Lodha, D.; Sharma, R.; Verma, U.; Dixit, J.; Balapure, A. K. Insulin Catalyzes the Curcumin-Induced Wound Healing: An In Vitro Model for Gingival Repair. *Indian J. Pharmacol.* **2012**, *44*, 458−462.

(74) Bullock, J. J.; Mehta, S. L.; Lin, Y.; Lolla, P.; Li, P. A. Hyperglycemia-Enhanced Ischemic Brain Damage in Mutant Manganese SOD Mice is Associated with Suppression of HIF-1α. *Neurosci. Lett.* **2009**, *456*, 89−92.